# Novel nanoliposomes synergistically modulated by sitogluside and dioscin: stability, bioavailability and capacity to alleviate hyperuricaemia

Gaodan Liu[1], Jingjian Liu[1], Ping Shao[1,2], Dan Kai[3,4], Liuqing Yang[5], Peilong Sun[1,2]*, Simin Feng[1,2]*

1.Department of Food Science and Technology, Zhejiang University of Technology, Hangzhou 310014, Zhejiang, People's Republic of China

2. Key Laboratory of Food Macromolecular Resources Processing Technology Research (Zhejiang University of Technology), China National Light Industry, Hangzhou 310014, Zhejiang, People's Republic of China

3. Institute of Materials Research and Engineering (IMRE), Agency for Science, Technology and Research (A*STAR), 2 Fusionopolis Way, Singapore 138634, Singapore

4. Institute of Sustainability for Chemicals, Energy and Environment (ISCE2), Agency for Science, Technology and Research (A*STAR), 1 Pesek Road, Jurong Island, Singapore 627833, Singapore

5. Department of TCM Gynecology, Hangzhou TCM Hospital Affiliated to Zhejiang Chinese Medical University, Hangzhou 310000, Zhejiang, People's Republic of China

Corresponding author:

Simin Feng, Department of Food Science and technology, Zhejiang University of Technology, Hangzhou 310014, Zhejiang, People's Republic of China. Tel: +86-18768118643

*E-mail: fengsimin@zjut.edu.cn

Peilong Sun, Department of Food Science and technology, Zhejiang University of Technology,

Hangzhou 310014, Zhejiang, People's Republic of China. Tel: +86-571-88320388

*E-mail: sun_pl@zjut.edu.cn

**ABSTRACT:** Cholesterol (Cho) is commonly used to stabilize nanoliposomes, however, there is controversy on the relationship between Cho and health. In this study, we developed a novel multifunctional nanoliposome utilizing structurally similar sitogluside (SG) and dioscin (Dio) instead of Cho to anchor the phospholipid bilayer and synergistically modulate the membrane properties of the nanoliposome (DPPC or DOPC). The storage and gastrointestinal tract stability experiment demonstrated that the changes of physical and chemical properties, including significantly reduced size and Dio retention rate of SG and Dio synergistically modulated nanoliposomes compared to those of SG alone regulated nanoliposomes. Moreover, the stabilization effect of DPPC nanoliposomes under the synergistically modulated of SG and Dio was superior to that of DOPC nanoliposomes. Similarly, in cell internalization and permeability studies, DPPC-sitogluside-dioscin (P-SG-Dio), which was synergistically modulated by SG and Dio, had the highest cellular uptake and transepithelial transport. In addition, compared with DPPC-cholesterol-dioscin (P-Cho-Dio) and free Dio, intragastric administration of P-SG-Dio for 14 days could effectively inhibit the activation of NLRP3 inflammatory in the kidney of hyperuricemia mice, exhibiting the best anti-hyperuricemia and anti-inflammatory effects. Fourier transform infrared spectroscopy and Raman spectroscopy results indicated that the glucose residues of SG and Dio synergistically modulate the membrane properties of nanoliposomes by forming hydrogen bonds between them and the polar heads of phospholipids. The absence of unsaturated bonds in DPPC led to the best effect of synergistic modulation, resulting in superior membrane properties, stability and bioavailability of P-SG-Dio. The finding offers valuable insight into the design and modification of nanoliposome for the effective delivery of bioactive compounds.

**Keywords:** delivery system, stabilizer, bioavailability, hyperuricemia, NLRP3 inflammasome

## 1. INTRODUCTION

With alterations in lifestyle, the prevalence of hyperuricemia is rapidly increasing worldwide[1]. Hyperuricaemia is mainly induced by elevated uric acid (UA) levels, impaired renal excretion of UA, or a combination of these mechanisms. It is a significant risk factor for diabetes, cardiovascular disease, chronic kidney disease, and metabolic syndrome. Hence, decreasing the production and promoting the excretion of UA is the mainstay of treatment for hyperuricaemia[2]. In the formation of UA, xanthine oxidase (XOD) is the critical enzyme engaged in the conversion of xanthine and hypoxanthine to UA. Conditions such as excessive consumption of purine-rich foods and a lack of genetic enzymes may result in uricemia and hyperuricemia[3]. Additionally, the NLRP3 (NLR family pyrin domain containing 3) inflammasome is a dangerous factor for inflammation and plays an important role in the pathogenesis of kidney inflammation. Excessive amounts of UA and oxidative stress can activate NLRP3 inflammasome, which in turn mediates the production of IL-1β and activates immune against danger signals[3]. Thus, suppressing the activation of NLRP3 inflammasome is a viable strategy to inhibit kidney inflammation. Benzbromarone (BEN) is a commonly used clinical drug for controlling serum UA levels, but it has side effects such as hepatic steatosis and limitations in patients with kidney dysfunction[4]. Therefore, it is essential to develop less toxic and more effective food active ingredients for the treatment of hyperuricemia, which provides a safer and sustainable solution for the disease management of hyperuricemia.

Dioscin (Dio) is a spirostane glycoside and natural steroidal saponin with a wide range of pharmacological activities, including anti-inflammatory, anti-cancer, hypolipidemic, anti-viral, anti-allergic, and anti-hyperuricemic effects[5]. Due to these properties, it has been extensively utilized in the functional food and pharmaceutical industries. Studies have shown that Dio extracted from *dioscorea*

*spongiosa* showed serum UA reducing effect in potassium oxonate induced hyperuricaemic mice[5]. However, the oral administration of Dio presents challenges such as hemolytic toxicity and poor aqueous solubility, which reduce its bioavailability and limit its therapeutic applications[6]. By incorporating Dio into variety of lipid based nanocarriers such as nanoemulsions, nanoliposomes, and nanostructured lipid carriers is an effective means to overcome the limitations of solubility, toxicity and bioavailability of Dio[7]. Among these, nanoliposomes have gained widespread attention and application due to their high low toxicity, biocompatibility, and non-immunogenicity[8]. Nanoliposomes are lipid bilayer colloidal vesicles in the nano-size range which can strengthen the stability of active compounds both *in vitro* and *in vivo*, and can enhance their absorption and bioavailability. However, there are limited reports on the encapsulation of Dio by nanoliposomes[9]. Therefore, the development of Dio-loaded nanoliposomes not only overcomes the problem of its low bioavailability, but also provides innovative carriers and technical support for the development of Dio in the field of drugs and food.

Cholesterol (Cho), a commonly used membrane stabilizer, plays a crucial role in regulating membrane fluidity and polarity[8]. However, high levels of Cho intake raise the risk of many diseases, including peripheral vascular disease, stroke, and coronary heart disease, restricting the clinical application of nanoliposome[6]. Thus, it is necessary to develop a novel nanoliposome delivery system that can effectively address these problems. To overcome this problem, we used phytosterols containing different C3 branched instead of Cho to anchor the phospholipid bilayer of nanoliposomes in our previous study[8]. We found that inserting sitogluside (SG) into the lipid bilayer enhanced the rigidity, stability, and bioavailability of the nanoliposomes. SG, a natural sitosterol glucoside, is a phytosterol present in many plants, which have potential pharmacological properties such as immunomodulatory, neuroprotective, anti-cancer and antioxidant[10]. Similar structural frameworks are present in the structures of SG and Cho,

thus SG has the ability to regulate the rigidity of the lipid bilayer and membrane stability[8]. In fact, the similar structure of Dio and SG inspired us to encapsulate Dio into the lipid bilayer to synergistically regulate the properties of the lipid bilayer with SG. Recently, it has been reported that the combination of two active ingredients synergistically modulating nanoliposomes could effectively improve their membrane stability and bioavailability and therapeutic effects[6, 11-13]. Zhu et al[11]. used ginsenoside Rg3 combined with paclitaxel to synergistically regulate the properties of liposomes, which made liposomes effectively kill tumors, regulate brain-tumor microenvironment, activate immune microenvironment in glioma, and thus significantly improve the anti-tumor effect. Thus, there is great potential for SG and Dio to synergistically modulate the properties of nanoliposomes.

Based on the excellent physicochemical properties and pharmacological activities of Dio and SG, and in order to overcome the limitations faced by traditional nanoliposomes, we creatively developed a novel nanoliposome using structurally similar SG and Dio to anchor phospholipid bilayers. Their feasibility as membrane stabilisers was investigated by differential scanning calorimetry (DSC), Fourier transform infrared spectroscopy (FTIR) and Raman spectra. The effects of SG and Dio synergism on the storage stability of nanoliposomes at different temperatures (4, 25, 37 °C) and *in vitro* simulated gastrointestinal digestion were investigated. Then, the bioavailability of nanoliposomes was verified by trans-epithelial cell monolayer transport assay. Finally, a hyperuricemia model was established to evaluate the therapeutic effect of nanoliposomes on hyperuricemic mice as well as to explore the mechanism of UA reduction and improvement of kidney inflammation. To the best of our knowledge, this is the first report exploring the effect of SG and Dio synergistic modulation of nanoliposome bilayers on their stability and bioavailability as well as on their uric acid-lowering effect. The findings presented in this study can be used as a basis for designing and optimizing nanoliposome delivery systems to open

new horizons for food active compounds in the food industry.

## 2. MATERIALS AND METHODS

### 2.1 Chemicals and reagents

Analytical grade chemicals dioscin (HPLC≥98%) and sitogluside (SG) were purchased from Shanghai yuanye Biotechnology Co., Ltd (Shanghai, China). 1,1'-dioctadecyl-3,3,3',3'-tetramethylindocarbocyanine perchlorate (DiI) were purchased from Shanghai Titan Scientific Co., Ltd (Shanghai, China). 1,2-dipalmitoyl-sn-glycero-3-phosphocholine (DPPC), 1,2-dioleoyl-sn-glycero-3-phosphocholine (DOPC), 1,2-dioleoyl-3-trimethylammoniumpropane (DOTAP) were purchased from AVT Pharmaceutical Tech CO., Ltd (Shanghai, China). Cell Counting Kit-8 (CCK-8) was obtained from Beijing Solarbio Science & Technology Co., Ltd (Beijing, China). 4',6-diamidino-2-phenylindole (DAPI) was purchased from Merck KGaA (Darmstadt, Germany). The UA, XOD, creatinine (CRE), blood urea nitrogen (BUN), malondialdehyde (MDA), superoxide dismutase (SOD), glutathione peroxidase (GSH-Px) texting kits were obtained by Nanjing Jiancheng Bioengineering Institute (Nanjing, China). Enzyme-linked immunosorbent assay (ELISA) kit of IL-1β and IL-18 ELISA kit was purchased from CUSABIO (Wuhan, China). RNAiso Plus reagent, PrimeScript™RT reagent kit, SYBR Green PCR Master Mix and primary antibodies against NLRP3, caspase1, ASC, IL-1β were obtained by Wuhan Servicebio Technology Co., Ltd (Wuhan, China). Other chemicals were all of analytical grade.

### 2.2 Preparation and characterization of nanoliposomes

The preparation of nanoliposomes was based on the thin film dehydration-rehydration method described previously with some modifications[8]. The lipid compositions (mol %) of DPPC-cholesterol

(P-Cho), DPPC-sitogluside (P-SG), DOPC-cholesterol (O-Cho), DOPC-sitogluside (O-SG) nanoliposomes were DPPC/DOTAP/Cho (65/10/25), DPPC/DOTAP/SG (65/10/25), DOPC/DOTAP/Cho (65/10/25), and DOPC/DOTAP/SG (65/10/25), respectively. Dio-loaded nanoliposomes were further prepared, in which the mass ratio of SG to Dio was (mSG:mDio)15:0, 15:2.5, 15:5, 15:7.5, 15:10, 15:12.5, 15:15. DiI fluorescently labeled nanoliposomes were prepared by adding 2 mol% DiI to the total lipids. Approximately 15 μmol lipids were dispersed in a moderate amount of chloroform/anhydrous ethanol mixture with a volume ratio of 1:5, and blended in a 50 mL round-bottom flask. The chloroform/ethanol mixture was removed by evaporation in a rotary evaporator (Rotavapor R-210, Büchi, Switzerland) under vacuum at 50 ℃ for 1 h to form a thin and uniform film. Then, the resulting lipid film was dried in a vacuum desiccator overnight to remove residual solvent. Then, they were rehydrated with 5% w/w aqueous glucose solution (pH 5.3) to give a final total lipid concentration of 10 mM. After mechanical stirring and sonication (5 min each) at 70 ℃ (50 ℃ for films containing DOPC), the solution was sized by 10 extrusions at 70 ℃ via a mini-extruder (Avanti Polar Lipids) attached to a 200 nm pore size membrane (Whatman Nucleore TM, GE Healthcare, Little Chalfont, U.K.). The mean particle diameter and particle size distribution of nanoliposomes were determined at 25 ℃ using particle size analyzer (Zetasizer nano-ZS Model Omni, Brookhaven Instruments Co.) under the dynamic light scattering (DLS) particle size measurement mode. The ζ-potential was measured using the same instrument under the ζ-potential measurement mode. The 10 mM nanoliposomes suspension were diluted to 1 mM with 5% w/w aqueous glucose solution, which were used to measure the mean particle diameter and particle size distribution and ζ-potential. In addition, transmission electron microscopy (TEM) (HT7700 Exalens, Hitachi, Japan) was applied to investigate the microstructure of DPPC-sitogluside-dioscin (P-SG-Dio) and DOPC-sitogluside-dioscin (O-SG-Dio) nanoliposomes with

158 SG:Dio=15:7.5.

159 **2.3. Determination of encapsulation efficiency (EE)**

160 The Dio encapsulation efficiency (EE) was determined according to a previously described method
161 with some modification[6]. Specifically, the nanoliposomes suspension were centrifuged at 4 ℃ and 13000
162 g for 1 h, and the unencapsulated dioscin in the supernatant was measured for absorbance at 550 nm
163 using a spectrophotometer (P7, Shanghai Meipuda Instrument, Ltd, China). The amount of free Dio was
164 determined using a standard curve ($Y = 1.0129x + 0.0014$, $R^2 = 0.9994$), and the EE were calculated
165 using eqs 1:

166 $$EE\% = \frac{\text{total Dio (mg)} - \text{unencapsulated Dio (mg)}}{\text{total Dio (mg)}} \times 100\% \quad (1)$$

167 **2.4. Structural analysis**

168 **2.4.1Differential scanning calorimetry (DSC)**

169 DSC was performed to characterize the thermal properties of nanoliposomes by using a TA Q20
170 DSC instrument (Waters). About 5-10 mg of nanoliposome samples were placed in aluminum pans,
171 which were then hermetically sealed and heated from 20 to 90 ℃ (-30 to 30 ℃ for membranes with
172 DOPC) at 1 ℃/min with a nitrogen flow of 50 mL/min. The empty aluminum pan was used to a reference.

173 **2.4.2 Fourier transform infrared spectroscopy (FTIR)**

174 In order to determine the interactions between SG, Dio and phospholipids (DOPC, DPPC and
175 DOTAP), infrared spectra were measured using an FTIR spectrometer (Nicolet iS50, Thermo) fitted with
176 a KBr beam splitter and KBr detector. The infrared spectra were obtained at 500-4000 $cm^{-1}$ for 32 scans
177 at a resolution of 2 $cm^{-1}$.

178 **2.4.3 Raman spectra**

179 A 10 μL sample of nanoliposomes were transferred to the glass slide. A 20x objective was used to

focus the laser beam on the convex spherical droplets. Measurements were performed using a confocal high-resolution Raman spectrometer equipped with a He-Ne laser (Horiba LabRAM HR Evolution, Japan). The Raman spectrometer was operated at a wavelength of 785 nm, with a laser power of 30 mW at the sampling point and an exposure time of 5 s. The axial and lateral resolutions obtained were 300 nm and 2.8 μm, respectively.

### 2.5 Stability evaluation

#### 2.5.1 Temperature stability

The average particle size and retention rate of Dio of nanoliposomes were measured at 4 ℃, 25 ℃, and 37 ℃ during 30 days of storage.

#### 2.5.2 *In vitro* simulated digestion stability

The digestive stability of nanoliposomes was evaluated by a method previously described by Liu et al[14]. The simulated gastric fluid (SGF) and intestinal fluid (SIF) were prepared according to Table S1. The nanoliposome dispersion was mixed with the digestive solution in a ratio of 1:1 (v:v). The SGF phase lasted for 2 h and the SIF stage continued for 4 h. After each stage of sample digestion, the reaction was terminated by centrifugation at 5000 g for 6 min and the supernatant was obtained for the next stage of the digestion experiment. Throughout the digestion stage, the sample was incubated at 37 ℃ with a rate of 100 r/min, then a 1 mL aliquot of each sample was taken every 30 min and centrifuged at 13000 g for 1 h for Dio relative release rate determination. The DLS method was used to record the changes in size, PDI and ζ-potential of the nanoliposome supernatant after centrifugation at 5000 g for 6 min. The cumulative release rate (%) of Dio was calculated using eqs 2:

$$\text{Cumulative release rate (\%)} = \frac{m_t}{m_0} \times 100\% \quad (2)$$

Where $m_0$ was the initial amount of Dio in nanoliposomes, $m_t$ was the cumulative amount of released

Dio at each time point during digestive stage.

**2.6 Cell studies of nanoliposomes**

**2.6.1 Cytotoxicity and cellular uptake study of nanoliposomes**

The cytotoxicity of nanoliposomes to Caco-2 cell was determined by the CCK-8 assay. Caco-2 cell was seeded at the density of $10^5$ cell/mL into 96-well plates and then incubated for 24 hours. The concentration of Dio or SG in the nanoliposomes (P-SG, P-SG-Dio, P-Cho-Dio, O-SG, O-SG-Dio, O-Cho-Dio) was varied from 0.3125 to 40 μg/mL at eight different values, with three wells for each value. The 10 μL of CCK-8 solution was added to the well and incubated at 37 ℃ with 5% $CO_2$ for 4 h. Following this, the optical density (OD) was determined at 450 nm. Caco-2 cells were seeded in 6-well plates at a density of $2\times10^4$ cell/well and then incubated for 24 h for cell uptake study. DiI fluorescence-labeled nanoliposomes with Dio concentration of 2.5 μg/mL were added, and the Caco-2 cells were incubated for 3 h at 37 ℃. The cells were then washed three times with 500 μL of PBS and fixed with 300 μL polyformaldehyde for 15 min. DAPI solution was added to the well, incubated at 37 ℃ for 10 min, and then washed with 500 μL PBS twice. Subsequently, the nanoliposomes were visualized via confocal laser scanning microscopy. The cellular uptake of Caco-2 cells was quantified by flow cytometry (ACEA NovoCyte, China) according to the previous method[8], and the resulting data was analysed using Flowjo software.

**2.6.2 Transepithelial transport experiments**

For transport experiments, 0.5 mL of DMEM contained $1\times10^5$ Caco-2 cells was seeded in the upper chamber of each well of 12-well transwell inserts. The culture medium of both compartments was replaced with a new one every 2 days for a total of 3 weeks. Cells developed to form dense monolayers when the transepithelial electrical resistance (TEER) value on the AP side of the transwell plate was >400

Ω·cm$^2$[15]. Caco-2 monolayer integrity was monitored by Millicell ERS-2 (Millipore Corporation) on days 3, 6, 9, 12, 15, 18 and 21. On the 21st day, the integrity of the cell monolayer was demonstrated indirectly using apparent permeability coefficient ($P_{app}$) value of lucifer yellow via the method of yang et al[15]. In order to assess the growth and differentiation properties of Caco-2 cells, an alkaline phosphatase kit was used to detect the enzyme activities on the AP side and BL side on days 7, 14 and 21. After 21 days of incubation, 0.5 mL and 1.5 mL of HBSS were then added to the AP side and BL side and equilibrated for 30 min before removing the HBSS. For AP to BL transfer, a sample containing 0.5 mL of HBSS (corresponding to 2.5 μg/mL Dio) was added to AP side and 1.5 mL of blank HBSS was added to BL side. After 3h, 200 μL of the sample was taken from the receiver compartment for analysis.

The $P_{app}$ was calculated using eqs 3:

$$P_{app} = \frac{\frac{dQ}{dt}}{A \times C_0} \quad (3)$$

where dQ/dt presented the transport rate in the receiver compartment (μg/s), A presented the membrane surface area of the transwell insert (1.12 cm$^2$), $C_0$ presented the initial Dio concentration in the donor compartment (μg/s).

**2.7 Animal experiments**

48 male Kunming mice (20±2 g) were purchased from Hangzhou Qizhen Laboratory Animal Science and Technology Co Ltd (permission number: SYXK 2022-0026). Mice were kept under specific pathogen free (SPF) conditions for 1 week of environmental acclimatization in a controlled room at a temperature of 25±1℃ and 50±10% humidity under a 12-hour light/dark cycle. All mice had free access to laboratory diet and water. This study was approved under the guidance of the Animal Ethics Committee of Zhejiang University of Technology (Ethics Number: MGS20230711097). The mice were randomly divided into 6 groups: normal control group, NC; model group, MOD (potassium oxonate, 200 mg/kg/d

BW + Hypoxanthine, 100mg/kg/d BW); positive control group, BEN (50 mg/kg/d BW); free Dio group, Dio (50 mg/kg/d BW); P-Cho-Dio group (40 mg/kg/d BW); P-SG-Dio group (40 mg/kg/d BW), with 8 mice per group. The model drug and free Dio were dissolved in 0.5% carboxymethyl cellulose sodium (CMC-Na) aqueous solution. Mice in the experimental group were first intraperitoneally injected with potassium oxonate at 8 a.m. each day, and one hour later, was given hypoxanthine by gavage. The NC group received gavage treatment with 0.5% CMC-Na aqueous solution. Hyperuricaemia was induced for 14 consecutive days. After one hour of gavage with hypoxanthine, mice in the BEN group, Dio group, P-Cho-Dio group, and P-SG-Dio group received the corresponding drug by gavage. Mice were all sacrificed at the end of day 21, then blood samples were collected. Blood samples were centrifuged at 3000 rpm at 4 ℃ for 5 min, and stored at 4 ℃ for analysis. Kidney and liver tissues were rapidly removed, washed with saline, and weighed. Then, kidney was divided into two parts, one was used to fix in 4% paraformaldehyde for histopathological analysis, and the other was saved at -80 ℃ for biochemical analyses. The kidney index and liver index were calculated using eqs 4 and 5:

$$\text{Kidney index (\%)} = \frac{\text{weight of kidney (mg)}}{\text{body weight (g)}} \times 100\% \quad (4)$$

$$\text{Liver index (\%)} = \frac{\text{weight of liver (mg)}}{\text{body weight (g)}} \times 100\% \quad (5)$$

**2.8 Serum and liver biochemical analysis**

Serum levels of UA, XOD, SCr, BUN and liver levels of XOD were determined using commercial detection kits following the manufacturer's instructions.

**2.9 Histopathological analysis**

Kidney tissue was fixed with 4% paraformaldehyde for 24 h and then embedded into paraffin. Using a standard method, kidney tissue sections about 4 μm were stained with hematoxylin and eosin (HE) for histopathological analysis. Then, the histological lesions of the kidneys were examined under a light

268 microscope (NIKON, Japan) at 200× magnification. Kidney injury was evaluated according to a
269 previous publication[3].

270 **2.10 Antioxidant activity and cytokine level**

271 The levels of MDA, SOD and GSH-PX in serum were measured using commercial detection kits
272 and the activities of IL-1β and IL-18 in serum and kidney were detected using enzyme-linked
273 immunosorbent assay (ELISA) kits. The test method was carried out according to the manufacturer's
274 instructions.

275 **2.11 Immunohistochemistry (IHC)**

276 Immunohistochemical staining was carried out as previously described[3]. Section was incubated
277 using IL-1β antibody (1:200, Proteintech, Wuhan, China) at 4℃ overnight. Next, they were incubated
278 with HRP-conjugated secondary antibody (Tuling Biomedical Co., Ltd, Hangzhou, China) for 1 h. The
279 levels of IL-1β in renal tissues was analyzed by microscopy (NIKON, Japan).

280 **2.12 Gene expression**

281 Total RNA was extracted from kidney using a total RNA isolation kit (Saiweier Biotechnology Co.,
282 Ltd, Wuhan, China). RNA concentration was determined using Nanodrop 2000 (Thermo Scientific).
283 Reverse transcription was carried out using a PrimeScript$^{TM}$RT reagent kit (Takara Bio, Shiga, Japan).
284 The cDNA was magnified using SYBR Green PCR Master Mix, and specific primers using the CFX96
285 Real-Time PCR Detection System (Bio-Rad, USA) and these primers were presented in Table 1. RT-
286 PCR was carried out in the CFX96 Real-Time PCR Detection System (Bio-Rad, USA). The relative
287 mRNA levels of NRLP3, ASC, caspase1 and IL-1β were quantified by the $2^{-\triangle\triangle Ct}$ method. β-actin was
288 used as a housekeeping gene.

289 **2.13 Western Blotting**

The renal tissues were homogenised using radioimmunoprecipitation assay (RIPA) lysis buffer including 0.1% phenylmethylsulfonyl fluoride (Saiweier Biotechnology Co., Ltd, Wuhan, China). The protein concentrations were then determined using bicinchoninic acid (BCA) (Saiweier Biotechnology Co., Ltd, Wuhan, China) kit. The protein extracts and the loading buffer were mix together in a ratio of 4:1 and boiled for 6 min. The mixtures were separated on an 8-10% SDS-PAGE gel and then transferred to a PVDF membrane (Saiweier Biotechnology Co., Ltd, Wuhan, China) for 1.5 h. The membranes were blocked for 1h at ambient temperature with 1% milk dissolved in Tris-buffered saline/Tween (TBST). They were incubated with antibodies against ASC (Proteintech, Wuhan, China), NLRP3 (Proteintech, Wuhan, China), caspase1 (Proteintech, Wuhan, China) and IL-1β (Proteintech, Wuhan, China) at a ratio of 1:1000 at 4℃ overnight. Subsequently, the membranes were incubated with the secondary antibodies (Proteintech, Wuhan, China) at an ambient temperature for 1h, following three washes with TBS-Tween. The protein bands were imaged with an enhanced chemiluminescence (ECL) kit (Proteintech, Wuhan, China), and quantified was performed using Image J software.

**2.14 Molecular Docking**

The binding affinity of Dio with the core target of liver injury core target was identified through molecular docking. p38α, the predominant isoform of p38 MAPK, exerts a pivotal role in the pathogenesis of liver injury. The three-dimensional structural model of p38α (PDB identifier 5OMH) was obtained from the Protein Data Bank (PDB) repository. The progression of docking was carried out in accordance with the methodology previously described[16], and a docking score of less than 8 points was taken to indicate low toxicity in the liver.

**2.15 Statistical Analysis**

The data were displayed as mean ± standard deviation and analyzed using one-way analysis of

variance (ANOVA), followed by Duncan's new multiple range test among multiple groups. A significance level of $p < 0.05$ was set for all of the tests.

## 3. RESULTS

### 3.1. Characteristics of Nanoliposomes

The characteristics of DPPC or DOPC nanoliposomes with different SG to Dio ratios (from 15:0 to 15:15) were shown in Figure 1. The particle size of DPPC and DOPC nanoliposomes increased with the addition amount of Dio (Figure 1A, B). This was because the dimensional occupation of Dio in nanoliposome membranes and increasing rigidity in lipid bilayer[8]. Nanoliposomes with PDI < 0.3 were deemed to have high stability, monodisperse and homogeneity[13]. For DPPC and DOPC nanoliposomes, PDI was all less than 0.3 and positively correlated with the amount of Dio addition, indicating that they had a narrow size distribution (Figure 1A, B). The positive charge on the surface of the nanoliposomes is due to the incorporation of the cation DOTAP. As shown in Figure 1(D, E), the electrical properties of nanoliposomes increased slowly with the addition of Dio, which due to the synergistic modulation of the lipid bilayer by SG and Dio reduced the electrostatic repulsion between the head groups, stabilized the bilayer, and generated a stable high potential[13, 17]. As shown in Figure 1(G, H), with the increase of Dio content, the EE of Dio-loaded nanoliposomes increased and then gradually decreased. When the ratio of SG to Dio was 15:7.5, the EE of DPPC and DOPC nanoliposomes was the highest, which was (83.31±1.92)% and (78.51±0.99)%, respectively. Therefore, the SG to Dio ratio of 15:7.5 was used for the next characterization. In terms of appearance (Figure 1C), P-SG, P-SG-Dio, O-SG, O-SG-Dio, suspensions were optically clear and no significant deposits. However, the turbidity of P-SG-Dio and O-SG-DIO suspension is higher than P-SG and O-SG, respectively. This may be due to the addition of Dio, increased the size of nanoparticles, and increased light scattering. Figure 1 (F, I) showed that P-SG-Dio,

O-SG-Dio had monomodal particle size distributions. The micromorphology of P-SG-Dio, O-SG-Dio was analyzed by TEM. It was observed that P-SG-Dio, O-SG-Dio had a uniform and near-spherical vesicles. Besides, TEM results showed the lower average diameters of P-SG-Dio, O-SG-Dio compares to DLS method. The DLS results represented the hydrodynamic size of nanoliposome in the swollen state, and TEM results showed the size of nanoliposome in the dried state[18].

### 3.2. Structural analysis

#### 3.2.1 Differential scanning calorimetry analysis

DSC can effectively reflect the chemical composition and physical state of nanoliposomes and capture the information about the intermolecular interaction between drugs and bilayer membranes[19]. At the ambient temperature, the pure DOPC nanoliposomes present in the liquid phase, and the pure DPPC nanoliposomes show in the gel phase[20]. The molecular arrangement of the phospholipid layer and the intermolecular interaction strongly affects the enthalpy of phospholipid phase transition[21]. It is reported that 33.5 ℃ is the pretransition temperature of pure DPPC vesicles (lamellar gel phase → rippled gel phase, $L_{\beta'} \rightarrow P_{\beta'}$), while 41.2 ℃ is its main transition temperature (rippled gel phase → lamellar liquid-crystalline phase, $P_{\beta'} \rightarrow L_{\alpha}$)[22]. After DOTAP is inserted into the phospholipid layer of pure DPPC, the pretransition peak vanished, and the main transition temperature of DPPC-DOTAP became 67.07 ℃, which changed the molecular arrangement of the phospholipid layer (Figure 2A). The stepwise addition of SG and Dio resulted in different main transition temperatures for the nanoliposomes. Compared to DPPC-DOTAP (67.09 ℃), the main transition temperatures of P-SG and P-SG-Dio were increased to 69.06 and 71.41 ℃. Dio insertion into P-SG further increased the intermolecular force. For pure DOPC vesicle, the phase transition changes from $L_{\beta}$ to $L_{\alpha}$ (gel to fluid) at the temperature of -20 ℃. As shown in Figure 2B, the main transition temperature of DOPC-DOTAP was higher (-0.90 ℃) than that of DOPC

vesicle. After inserting SG and Dio, the main transition temperature of O-SG, O-SG-Dio shifted to lower values, and the peaks broadened to varying degrees. The main transition temperature of O-SG was reduced to -13.71 ℃, which was higher than O-SG-Dio (-14.73 ℃). This suggested that Dio insertion into O-SG further increased change in the structure of the phospholipid layer[21].

### 3.2.2 Fourier Transform Infrared Spectrogram Analysis

The wavenumber changes of nanoliposomes were analyzed by FTIR. A pair of peaks appeared around 2800-3000 $cm^{-1}$ for the symmetric (~2850 $cm^{-1}$) and asymmetric (~2920 $cm^{-1}$) stretching vibration of the C–H bond of $CH_2$. The relatively strong band located at 1735 $cm^{-1}$ is attributed to the stretching vibration of C=O from the ester carbonyl group. In addition, the polar head group has three spectral bands in the asymmetric stretching vibration of N-$CH^{+}_3$ (~970 $cm^{-1}$), the symmetric stretching vibration of $PO^{2-}$ (~1090 $cm^{-1}$) and the asymmetric stretching vibration of $PO^{2-}$ (~1250 $cm^{-1}$)[23-25]. As shown in Figure 2C, D, the absorption peak at 3420 $cm^{-1}$ was attributed to –OH stretching[21], and the addition of Dio shifted the –OH stretching absorption peak of P-SG-Dio, O-SG-Dio to 3432, 3443$cm^{-1}$, respectively. Besides, similar main peaks were found in the FTIR spectrum of nanoliposomes with DPPC or DOPC as membrane materials, demonstrating that the inserted SG and Dio did not undergo severe chemical reactions in the membrane. The symmetric and asymmetric stretching vibrations of $CH_2$ in DPPC and DOPC nanoliposomes were unchanged, which indicated that $CH_2$ divided itself from the intermolecular interaction. For DPPC nanoliposomes, the addition of SG to pure DPPC vesicles did not induce the stretching vibration of C=O, and further addition of Dio shifted the nanoliposomes to lower frequencies (Figure 2C). This may be due to interaction through hydrogen bond formation between the C=O group of the phospholipid and OH groups of Dio[23]. After SG insertion, a spectral move of $PO^{2-}$ (symmetric and asymmetric stretching vibrations) toward a lower frequency was shown in P-SG, which reflected the

formation of hydrogen bonds between the oxygen group of the phospholipid and the hydroxyl group of SG, and the enhancement of the oscillation strength of SG[26]. The symmetric stretching vibration of $PO^{2-}$ existed a blue shift to higher wavenumbers after the insertion of Dio Figure 2C. This might be because the insertion of Dio produced hydrogen bonds between the hydroxyl group of the glucose residue and $PO^{2-}$ of phospholipid head group[8]. Figure 2D shown that the wavenumbers of $PO^{2-}$ (only asymmetric stretching vibration) and $N\text{-}CH^{+}_{3}$ in O-SG all shifted to lower values, suggesting that the hydroxyl group of SG and $PO^{2-}$ and $N\text{-}CH^{+}_{3}$ of phospholipids are involved in the formation of hydrogen bonds. After further addition of Dio to O-SG, the wavenumbers of $N\text{-}CH^{+}_{3}$ in O-SG-Dio shifted to lower values, indicating that the groups of Dio interacted slightly with the phospholipid head groups.

### 3.2.3 Raman spectra

Raman spectroscopy can reflect the symmetric stretching vibration of the C-C choline group in nanoliposomes, and lateral packing order of lipid molecule[27]. The polar group of the phospholipid head was very sensitive to the load of the external components[24]. When the characteristic peak is mainly positioned between 710 and 720 $cm^{-1}$, the symmetric stretching vibration of the C-C in the choline group mainly assumed as a gauche conformation[24, 28]. In the 718, 1444, 2850, and 2880 $cm^{-1}$ recorded the intensity of the nanoliposome's spectrum, and $I_{718}/I_{1444}$ and $I_{2880}/I_{2850}$ represented the C-N symmetric stretching vibration of the nanoliposome head choline group and the interchain lateral ordering of lipid molecules, respectively. It can be seen from Figure 2E that the intensity of all nanoliposomes was around 718 $cm^{-1}$, indicating that the choline groups in the nanoliposome bilayer was gauche conformations. Research has shown that torsional vibration of $CH_2$ near 1444 $cm^{-1}$ is insensitive to conformational change in the polar head, thus $I_{718}/I_{1444}$ is used to manifest the effect of the polar head interaction of SG, Dio and nanoliposome on the twisted conformation of choline group[29]. As shown in Figure S1A, for

DPPC nanoliposomes, the $I_{718}/I_{1444}$ ratio of P-SG was significantly reduced after the addition of SG and the $I_{718}/I_{1444}$ ratio of P-SG-Dio decreased to the minimum after further adding Dio. This was due to the fact that SG and Dio both contained hydroxyl groups and there were more hydroxyl groups in Dio containing three of the glucose residues than in SG containing one of the glucose residue, which made the polar head of DPPC reacted more with these hydroxyl groups[23]. For DOPC nanoliposomes, the $I_{718}/I_{1444}$ ratio of O-SG formed by the addition of SG was significantly decreased, and The $I_{718}/I_{1444}$ ratio changed slightly with further addition of Dio. It indicated that the groups of Dio had a slight interaction with the groups of phospholipid head, which was consistent with the FTIR results. The overall $I_{718}/I_{1444}$ ratio of DPPC nanoliposomes was lower than that of DOPC nanoliposomes, suggesting that the hydroxyl groups of SG and Dio interacted with the polar head group of DPPC more strongly than those of DOPC.

The antisymmetric (~2880 $cm^{-1}$) and stretching vibration bands (~2850 $cm^{-1}$) of $CH_2$ belong to the C–H stretching region, which keenly respond to changes of alkyl chain conformations and the lateral order between chains (Figure 2F)[27]. The intensity ratio $I_{2880}/I_{2850}$ is used to respond to the degree of lateral packing order of lipid molecules in nanoliposomes. The lateral order of molecular arrangement is enhanced by the increase of the intensity ratio of $I_{2880}/I_{2850}$. As shown in Figure S1B, the $I_{2880}/I_{2850}$ of DPPC and DOPC nanoliposomes were gradually increased with the gradual insertion of SG and Dio into the lipid bilayer, indicating that the loading of SG and Dio could improve the arranged horizontal order and reduce membrane mobility of nanoliposomes. However, the changes of $I_{2880}/I_{2850}$ of DPPC and DOPC nanoliposomes were slight, which indicated that the hydrophobic steroid ring and nonpolar side chain of SG and Dio had weak hydrophobic interactions with the hydrophobic region of the bilayer. Therefore, SG and Dio regulated the stability of nanoliposomes mainly through the binding of hydroxyl groups and phospholipid head groups at the hydrophilic site, which was consistent with the FTIR results[24].

### 3.3 The stability of Dio-loaded nanoliposomes

#### 3.3.1 Stability of Dio-loaded nanoliposomes at different temperatures

It was reported that the generation of lipids free radicals and the oxidation of phospholipids increased with the rise of temperature[30]. At a high storage temperature, the liquidity and permeability of nanoliposomes have also increased, leading to its fusion and the increase of particle size. After 30 days storage, the size of P-SG, P-SG-Dio, O-SG, O-SG-Dio increased from 127.35±2.58, 144.98±2.14, 119.74±3.7, 137.24±2.34 nm to 150.78±1.4, 154.28±3.12, 147.89±2 and 156.28±2.66 nm under 4 ℃, respectively (Figure 3A). Dio retention was all above 90% in both DPPC and DOPC encapsulated systems at 4 ℃ (Figure 3D). However, after 30 days of storage, the size of P-SG and O-SG at 25 ℃ (162.94±1.4 nm and 165.51±2.61 nm, respectively) were close to those of P-SG-Dio and O-SG-Dio (159.41±4.11 nm,166.11±3.21 nm, respectively). Meanwhile, the size of P-SG and O-SG at 37 ℃ (173.93±2.48 nm and 182.91±2.64 nm, respectively) was significantly higher than that of P-SG-Dio and O-SG-Dio (169.47±1.93 nm, 177.73±3.54 nm, respectively). After 30 days of storage, the retention rate of P-SG-Dio at 25 ℃ (91.09±3.48%) and at 37 ℃ (82.55±2.9%) was observably higher than that of O-SG-Dio (85.23±2.99% at 25 ℃, 68.28±3.56% at 37 ℃) (Figure 3E, F). Interestingly, the rate of increase in particle size and the decrease in retention rate of P-SG-Dio tended to change slowly after storage for a period of time, suggesting its potential for storage stabilization.

#### 3.3.2 *In vitro* simulated digestion stability of Dio-loaded nanoliposomes

The changes in DPPC and DOPC nanoliposomes before and after simulated digestion were assessed by measuring the cumulative release of Dio, size, PDI and ζ-potential. As shown in Figure 3G, Dio in P-SG-Dio and O-SG-Dio released slowly within 2 h in SGF, and the cumulative release of Dio was all less than 10%, indicating that Dio-loaded nanoliposomes could withstand the destruction of gastric acid at

low pH. The considerable release of Dio in P-SG-Dio and O-SG-Dio was observed throughout the SIF digestion period, with a particularly explosive release in the first 2 hours. The cumulative release rate of Dio from P-SG-Dio and O-SG-Dio reached 69.1±1.61% and 85.5±2.95%, respectively, after 6 h of gastrointestinal digestion. This demonstrated that P-SG-Dio significantly improved Dio stability in simulated gastrointestinal tract. With the releasing of Dio, size and PDI have also increased significantly, while ζ-Potential decreased significantly (Figure 3H-J). The size, PDI and ζ-Potential of nanoliposomes with different formulations did not change drastically in the gastric phase, while they changed drastically in the intestinal phase. After SIF digestion for 4 h, the particle sizes of P-SG and O-SG (708±5.11 nm, 831.46±7.76 nm, respectively) were significantly larger than those of P-SG-Dio and O-SG-Dio (396.55±4.25) nm, (520.32±10.59) nm, respectively. Moreover, the PDI and ζ-Potential of P-SG (0.48±0.01, 22.49±2.1mV) and O-SG (0.5±0.02, 20.27±2.84 mV, respectively) were high to those of P-SG-Dio and O-SG-Dio (0.33±0.05, 28.77±2.54mV; 0.43±0.03, 25.28±0.79, respectively). The minimal changes in particle size, DPI, and ζ-potential of P-SG-Dio indicated that it was highly stable in simulating gastrointestinal digestion.

### 3.4 Cell studies of Dio-loaded nanoliposomes

#### 3.4.1 Biocompatibility evaluations and cell internalization profiles of Dio-loaded nanoliposomes *in vitro*

ISO 10993-5 specifies that the cell activity status greater than or equal to 80% is noncytotoxic[31]. As shown in Figure 4A, when the concentration of P-SG, O-SG, Dio-loaded nanoliposomes, SG, Dio and SG/Dio mix was 0.315-40 μg/mL, Caco-2 cell viability reduced in a dose-dependent manner. The Caco-2 cell viability of free SG, Dio and SG/Dio at concentrations of 0.315-40 μg/mL were all greater than 100%, which were significantly higher than those of P-SG, O-SG, and Dio-loaded nanoliposomes. This

was due to the fact that the poorly soluble free SG, Dio and SG/Dio mixes were limited to reach the cell surface in solution. The cell viability of P-SG-Dio was lower than that of other nanoliposomes at different concentrations, which exposed its excellent ability to be taken up by Caco-2 cell. The concentration of P-SG, O-SG, Dio-loaded nanoliposomes, SG, Dio and SG/Dio mix was 2.5 μg/mL, the activity of Caco-2 cell was all above 80%. Therefore, the concentration of 2.5 μg/mL was used in subsequent experiments. After treatment of Caco-2 cell with fluorescently labeled nanoliposomes, the uptake was quantified using flow cytometry and observed using CLSM (Figure 4B-C). It was observed that P-SG-Dio was internalized to a greater extent than other nanoliposomes. Notably, there was a significant difference in cellular uptake of DPPC and DOPC nanoliposomes, with DPPC nanoliposomes being taken up by cells to an overall higher extent (Figure 4A). The quantitative results of flow cytometry implied that the fluorescent intensity of DiI-labeled nanoliposomes was shown as follows: P-SG-Dio>P-Cho-Dio>O-SG-Dio>P-SG>O-Cho-Dio>O-SG (Figure 4B). The average fluorescence intensity of P-SG-Dio was 9294±406, which was higher than that of other nanoliposomes. The results of the quantitative analysis generally matched the results of the qualitative analysis.

**3.4.2 Transport across Caco-2 cell monolayers**

*In vitro* permeability studies are an effective method to assess the absorption enhancement effect of nanocarriers on the endothelial barrier[32]. TEER could be used to directly reflect the integrity of Caco-2 cell monolayer[33]. With the prolongation of incubation time, the TEER value of Caco-2 cell increased, and the TEER value was 434.8±19.77 $\Omega \cdot cm^2$ (more than $300\Omega \cdot cm^2$) on the 21st day, which indicated that the Caco-2 monolayer was dense and complete, and could be used for the next experiment[32]. The linear regression equation for lucifer yellow absorbance was $Y = 727.48x + 10.687$, $R^2 = 0.9992$ (Figure S2) and the permeability of lucifer yellow to Caco-2 cell was obtained as $2.78\times10^{-8}$ cm/s. Figure 4E

revealed that on day 21st, the alkaline phosphatase activity on the AP side was 6.64 times higher than that on the BL side. These results indicated that Caco-2 cell was complete differentiation and the monolayer was morphological integrity for subsequent experiments on the 21st day[33]. Figure 4F displayed the $P_{app}$ of free Dio, and Dio-loaded nanoliposomes across Caco-2 monolayers. Compared to free Dio, the $P_{app}$ value of Dio encapsulated by P-Cho-Dio, P-SG-Dio, O-Cho-Dio, and O-SG-Dio increased by 7.46, 11.79, 3.38, and 5.04-fold, respectively, which manifested nanoencapsulation significantly increased cellular transport of Dio. Furthermore, $P_{app}$ value of P-SG-Dio were remarkably higher than those of P-Cho-Dio, O-Cho-Dio and O-SG-Dio.

**3.5 Effects of Dio-nanoliposome on hyperuricemia and renal function in mice**

During the 2 weeks treatment, the average water consumption and body weight of each group were recorded simultaneously. The average water consumption of the mice in all experimental groups exhibited a notable decline from the third day onwards (except for the NC group), and rebounded significantly on the eighth day, and the average water consumption of P-SG-Dio increased the fastest (Figure 5A). The body weight of mice in all groups began to decrease on the sixth day (except for the NC group), indicating the successful modelling of the experiment. The body weight of mice in the MOD group decreased dramatically and was significantly lower than that of the from the NC group from sixth day onwards, whereas the body weights of mice in the BEN, Dio, P-Cho-Dio, and P-SG-Dio groups began to recover slowly from the ninth day onwards. The P-SG-Dio group exhibited the most rapid increase in body weight (Figure. 5B). The key enzyme XOD was strongly associated with the production of UA. As shown in Figure 5C, D, the serum and liver levels of XOD were dramatically higher in the MOD group compared with the NC group. However, administration of BEN, Dio or Dio-loaded nanoliposome markedly reduced XOD levels in serum and liver, and the therapeutic effects were

comparable in the BEN and Dio-loaded nanoliposome groups. Serum UA level was remarkably higher in MOD group (Figure. 5E) and significantly lower in BEN group as compared to NC group. Dio or P-Cho-Dio treatment had a slight effect on serum UA level, and P-SG-Dio group significantly reduced serum UA level compared with the MOD group. Serum BUN level was elevated in the MOD group compared to the NC group, whereas serum BUN level was significantly decreased between the treatment groups compared to the MOD group, with no notable difference between the treatment groups (Figure 5F). Furthermore, the SCr level was observed to be elevated in the MOD group in comparison to the NC group. P-SG-Dio significantly reduced SCr level in hyperuricemic mice (Figure 5G), and BEN treatment had a similar reduction effect. Kidney index was markedly higher in the model group. Kidney index of BEN, Dio, Dio-loaded nanoliposomes was significantly lower compared to model group (Figure 5H). Translation of hyperuricaemia-induced inflammatory cell infiltration and tissue damage into a histological severity score was used to assess kidney injury (Figure 5I). The pathological changes in each group were shown in Figure 5I, J. The kidney tissues of mice in the NC group exhibited normal morphology and lacked evidence of inflammation. The kidney tissues in the MOD group exhibited notable alterations, including thickening of the glomerular basement membrane, vacuolization of the glomerular epithelium, dilation of the renal tubules, and the presence of vacuoles within the renal tubules. BEN, Dio and Dio-loaded nanoliposome treatment obviously improved the above abnormal pathological states. P-SG-Dio treatment attenuated tubulointerstitial and glomerular lesions, in contrast to the other groups where varying degrees of damage existed.

**3.6 Effect of Dio-loaded nanoliposomes on cytokine production in serum and kidney tissues and oxidative stress injury in serum of hyperuricemic mice**

As shown in Figure 6A-D, the levels of IL-1β and IL-18 were markedly elevated in serum and

kidney of mice in the MOD group compared with those in the NC group. BEN, Dio, P-Cho-Dio or P-SG-Dio could notably reverse the elevation of IL-1β and IL-18 in serum and kidney tissues, and the inhibitory effects were as following: BEN > P-SG-Dio > P-Cho-Dio > Dio. There was no significant difference between the inhibitory effect of P-SG-Dio and that of BEN, indicating that P-SG-Dio could alleviate kidney injury by inhibiting the inflammatory response. Subsequently, the serum levels of MDA, prominent antioxidant enzymes (SOD, GSH-Px) were detected. Compared with the NC group, the serum levels of MDA were obviously increased and the levels of SOD and GSH-Px were markedly decreased in the MOD group (Figure 6E-G). However, P-SG-Dio could obviously reduce the MDA level, the reduction effect was not significantly different from that of BEN, and better than that of Dio, P-Cho-Dio. P-SG-Dio markedly enhanced the levels of SOD and GSH-Px, with the effect of elevating SOD being more pronounced than that of BEN. The findings demonstrated that P-SG-Dio could attenuate oxidative stress injury in hyperuricemic mice. IHC was used to detect the expression of inflammatory cytokine IL-1β. As shown in Figure 6H-I, high level of positive staining of inflammatory cytokine IL-1β was observed in the kidneys of MOD group. BEN, Dio, P-Cho-Dio or P-SG-Dio all notably reduced the expression of IL-1β, with P-SG-Dio having the best inhibitory effect, which was not obviously different from the inhibitory effect of BEN.

**3.7 Effect of Dio-loaded nanoliposome on NLRP3 inflammasome in hyperuricemic mice**

Studies have shown that the inflammatory cytokines IL-1β and IL-18 were downstream products of the NLRP3 inflammatory pathway[3]. The regulation of protein expression of NLRP3 inflammasome signal pathway by Dio-loaded nanoliposome was shown in Figure 7A-E. The protein expressions of IL-1β, NLRP3, ASC, and caspase1 were dramatically increased in kidney tissues of the MOD group compared to the NC group. BEN, Dio, P-Cho-Dio or P-SG-Dio reduced the protein expression levels of

NLRP3 inflammatory pathway to different degrees. The inhibition of protein expression of IL-1β, NLRP3, ASC and caspase1 by P-Cho-Dio or P-SG-Dio was slightly better than that of BEN, and P-SG-Dio had the best inhibition effect. Consistent with the protein expression results, mRNA expression of NLRP3, ASC, caspase1 and IL-1β was significantly reduced in kidney tissues of hyperuricemic mice treated with BEN, Dio, P-Cho-Dio or P-SG-Dio (Figure 7F-I), and the inhibitory effects were as follows: BEN > P-SG-Dio > P-Cho-Dio > Dio. The inhibitory effects of P-SG-Dio and BEN on the mRNA expression of NLRP3, ASC, caspase1 and IL-1β were similar. It indicated that Dio-loaded nanoliposome could reduce renal inflammation by inhibiting the activation of NLRP3 inflammasome.

**3.8 Effects of Dio on liver injury**

The effect of Dio on liver injury was studied (Figure S3). Liver index, ALT and AST indexes did not differ between the groups (Figure S3A-C). The binding activity between Dio and p38α was predicted by molecular docking (Figure S3D), and docking score of Dio to p38α was -7.8, suggesting low toxicity to liver[4].

## 4. DISCUSSION

The first step in developing Dio-loaded nanoliposomes as effective carriers for hyperuricemia therapy is to ensure that they exhibit physicochemical stability before and after administration[34]. The DLVO theory suggests that the energy content enclosed of particles within the nanoliposomes loaded with active ingredients will increase with the improving of temperature, enhancing the probability of the collision and aggregation of particles, issuing in the destruction of the nanoliposomes structure and active ingredients leakage[30]. However, the retention and particle size of Dio-loaded nanoliposomes did not change tempestuously with increasing temperature (Figure 3). This might be due to electrostatic repulsion caused by the high positive charge on the nanoliposome surface, which prevented the fusion and

aggregation of vesicles during storage[35]. P-SG-Dio showed the best storage stability after 30 days of storage at higher temperatures (25, 37 ℃), suggesting that the synergistically modulated of SG and Dio reduction of lipid membrane disturbances and fluidity, and had a stronger stabilizing effect on DPPC bilayer. In SGF, the low pH value could reduce the surface charge of all nanoliposomes and promote liposome aggregation and flocculation[30]. However, the properties of DPPC and DOPC nanoliposomes did not change tempestuously and the cumulative release of Dio was below 10%, suggesting that the DPPC and DOPC nano-loaded systems can effectively prevent the hydrolysis by pepsin as well as the effect of the high ionic strength and high acidity. The presence of compounds in SIF, such as anions, pancreatic enzymes, and bile salts, might cause hydrolysis of the outer lipid layer of the nanoliposome and the solubilization of bile salts, leading to the rupture of the nanoliposome structure[13, 30]. After SIF digestion, the sizes of the different formulations of nanoliposomes were maintained at the nanoscale level (less than 1000 nm), further demonstrating the high stability of DPPC and DOPC nanocarriers. The P-SG-Dio properties, which are synergistically regulated by SG and Dio, are minimally altered. Moreover, SG, Dio could fill up the pores formed instantly when bile salts dissolve the nanoliposome membranes in SIF, thus preventing the nanoliposomes from rupturing and aggregating [30, 36].

There are two possible pathways for nanocarriers to enter the epithelial cell layer: the paracellular pathway and/or endocytosis via a transcellular pathway[37]. The mechanism of nanoliposome entry depended on factors such as cell type and size, surface charge, and material composition of the nanoliposomes. The paracellular pathway was regulated by tight junctions between the enterocyte cells. Despite the complete opening of tight junctions, the width between the enterocyte only was 20 nm, whereas the particle sizes of Dio-loaded nanoliposomes (all greater than 100 nm) are larger than the width between the enterocyte, and thus the entry of nanocarriers into the cell through the paracellular

598 pathway was restricted[38]. For free Dio, paracellular and transcellular transport were possible modes of
599 entry into the cell. However, further studies were needed to verify this. Moreover, positively charged
600 nanoliposomes can destroy cell membranes via interacting with negatively charged sialic acid of the
601 mucus membrane, thereby facilitating the uptake and transport of bioactive compounds within the cell[7].
602 As a consequence, the cell permeability of DPPC and DOPC nanoliposomes was markedly greater than
603 that of free Dio (Figure 4F). The transcellular pathways by which nanoliposomes enter cells include
604 caveolae-dependent endocytosis, clathrin-dependent endocytosis, fusion and macrocytosis[23]. Previous
605 studies have revealed that positively charged DPPC nanoliposomes were taken up by Caco-2 cells via
606 energy-dependent endocytosis and that the efficiency of uptake was influenced by their rigidity[8, 39]. The
607 rigidity of nanoliposomes was closely related to their membrane material composition and property[40],
608 and the most rigid liposomes would show the greatest degree of cellular uptake[41]. It can be postulated
609 that SG and Dio synergistically modulate the DPPC bilayer following insertion into the lipid bilayer,
610 resulting in a gradual increase in the rigidity of the nanoliposomes and an enhanced capacity to enter the
611 cell. Moreover, SG and Dio not only reinforced the structural integrity of the DPPC lipid bilayer but also
612 incorporated glucose residues within the hydrophilic glycosidic chain, which served as a substrate for
613 glucose transporter proteins (GLUTs). Thus, the glucose residues of SG and Dio functioned perfectly as
614 ligands for GLUT, allowing GLUTs to enter Caco-2 cells via GLUT receptor-mediated endocytosis.[11, 12]
615 Conversely, DOPC nanoliposomes are readily deformable due to their liquid phase status at room
616 temperature. This enables them to enter cells via energy-independent membrane fusion[39], resulting in
617 low cell internalization and permeability[42].

618 This study demonstrated that P-SG-Dio had the ability to reduce UA synthesis and promoted
619 nephroprotective effects in hyperuricemic mice compared to free Dio and P-Cho-Dio. P-SG-Dio was as

effective as the clinical drug BEN in the treatment of hyperuricaemia, due to the enhanced stability and bioavailability of Dio. Hyperuricaemia resulted from an imbalance in the regulatory system of UA production and excretion. Maintaining serum UA to appropriate levels represented the most effective strategy for the treatment of hyperuricaemia[43]. XOD is an enzyme that catalyzes the production of xanthine from hypoxanthine and then UA, as well as the direct production of UA from xanthine. Excessive production of XOD enhanced serum UA concentration and induced hyperuricaemia[4]. Therefore, UA formation could be reduced by inhibiting XOD production. Our study showed that P-SG-Dio significantly reduced XOD production (Figure 5C, D). In UA excretion, more than 70% of UA was excreted via the renal route. Genome-wide association studies have shown that about 90% of patients with hyperuricaemia have inadequate excretion[3]. However, inadequate excretion of UA in the kidneys can cause renal inflammatory injury and further cut down their functions, which in turn aggravates the kidney dysfunction for UA excretion. BUN and CRE were important indices for detecting kidney damage[44]. Serum BUN and CRE levels were obviously reduced in the P-SG-Dio group of mice relative to the MOD group. The levels of inflammatory cytokines IL-1β and IL-18 in serum and kidney were further examined and P-SG-Dio dramatically reversed the elevation of pro-inflammatory cytokines in serum and renal tissues, suggesting that its nephroprotective action might be due to its anti-inflammatory effects. HE staining of kidney tissue showed notable pathological improvement, further validating its nephroprotective properties. High UA levels could activate NLRP3 inflammatory, which could promote the full maturation and secretion of IL-1β and IL-18, leading to kidney inflammation and further kidney injury[45]. The NLRP3 inflammasome was the complex of multiple proteins, containing NLRP3, the effector cysteine protease caspase1and the adaptor protein ASC. When NLRP3 was irritated by UA, induction of pro-caspase1 and cleavage of ASC were converted to its active form through the interactions

described above. Then, caspase1 led to the expression of inflammatory cytokine IL-1β[46]. Evidence suggested that oxidative stress can enhance oxidative enzymes to stimulate the growth of ROS, which might activate the NLRP3 inflammasome signal pathway to upregulate the production of pro-inflammatory cytokines of IL-1β and IL-18[47]. Oxidative stress injury can be inhibited by regulating the levels of antioxidant enzymes. In this study, P-SG-Dio markedly reduced MDA levels, notably enhanced SOD and GSH-Px levels, and attenuated oxidative stress injury (Figure 6E-G). Thus, P-SG-Dio inhibited activation of the NLRP3 inflammatory pathway by reducing UA production through inhibition of XOD production as well as reducing oxidative stress, thereby attenuating kidney injury in hyperuricemic mice.

SG and Dio played an important role in controlling membrane fluidity and permeability, and their own molecular structure affected the properties of the nanoliposomes they built (such as rigidity, stability, bioavailability, and efficacy)[6, 8]. Research has shown that SG was placed in the lipid bilayer in the following manner: the glucose residue at C3 interfaced with the hydrophilic head group of the lipid bilayer, the hydrophobic steroid ring was positioned parallel to the acyl chain of the lipid bilayer, and the C17 side chain was collinear with side chain of the hydrophobic fatty acid[48]. SG could restrict the movement of acyl chains of the phospholipid bilayer and anchor the choline ammonium group near the membrane surface through the interaction of SG at the C3 site with phospholipid hydrophilic head groups, which leaded to an increase in lipid membrane order and the rigidity of the nanoliposomes[49]. Likewise, Dio had a similar structure to SG, consisting of a hydrophilic glycosidic chain at the C3 site and a hydrophobic aglycones, so that it can embed the lipid bilayer in the same manner, and synergized with SG to regulate the order of lipid stacking in the lipid bilayer, and the size, rigidity, the surface state of the nanoliposomes[6, 12]. Our study showed that the insertion of SG significantly improved the stability, bioavailability and curative effect of the nanoliposomes. After further insertion of Dio, the stability,

664 bioavailability, curative effect of the nanoliposomes were dramatically improved and outperformed that
665 of conventional nanoliposomes (Cho nanoliposomes) (Figure 3, 4). FTIR and Raman results indicated
666 that the molecular interactions between SG and Dio with phospholipids mainly appeared between the C3
667 group and the hydrophilic head group. Furthermore, both SG and Dio had glucose residues at the C3 site,
668 and the hydroxyl group of the glucose residues could interact with the polar head group ($PO^{2-}$) of
669 phospholipids to form hydrogen bonds, which led to changes in the lipid bilayer packing geometrical
670 structure and an enhanced cohesion of the bilayer membrane, thus strengthening the stability of
671 membrane.[49, 50] Besides, since Dio had more hydroxyl groups with three glucose residues than SG with
672 only one glucose residue, the hydroxyl groups of Dio can form more hydrogen bonds with the oxygens
673 of phospholipids, which significantly increased the level of the in-plane lateral phospholipid packing
674 density and made its nanoliposome more rigid[12, 51]. Moreover, the hydroxyl group between SG and Dio
675 can also form hydrogen bonds, which further stabilizes the membrane properties[17]. Hence, the synergistic
676 effect of SG and Dio resulted in a dramatic increase in the stability, bioavailability and curative effect of
677 the nanoliposomes.

678 Our results demonstrated that DPPC nanoliposomes have higher stability and bioavailability than
679 DOPC nanoliposomes. This was primarily due to the different properties between DPPC and DOPC in
680 terms of carbon chain length, number of unsaturation, and phase state[20]. DOPC was in liquid phase at
681 environmental temperature due to two unsaturated 18-hydrocarbon chains, whereas DPPC was in gel
682 phase at environmental temperature due to two fully saturated 16-hydrocarbon chains[20]. The structural
683 difference of the lipid bilayers between liquid-phase DOPC and gel-phase DPPC was attributed to the
684 degree of unsaturation of the acyl chains. The unsaturation disrupts chain elongation and molecular
685 stacking, making DPPC bilayers more ordered, thicker, stiffer, and more stable than those of DOPC at

686 room temperature[20, 52]. This is further supported by our DSC results, which show that the main transition
687 temperature of DOPC nanoliposomes is generally lower than that of DPPC nanoliposomes (Figure 2A,
688 B). SG and Dio have different interactions with unsaturated or saturated phospholipid. The properties of
689 DOPC nanoliposomes are affected not only by the hydrogen bonding between the glucose residues of
690 SG, Dio and the hydrophilic head groups of DOPC, but also by the unsaturated double bonds in its acrylic
691 chains. The double bond of DOPC would disturb the stacking of hydrocarbon chains and damage the
692 cooperativity of chain interactions in phospholipid bilayer, resulting in a decrease in the rigidity of DOPC
693 bilayer[20,51]. In addition, the destabilizing effect of the unsaturated bonds in the acyl chain of DOPC on
694 the lipid bilayer was much greater than the stabilizing effect of the hydrogen bonds of SG and Dio on the
695 lipid bilayer, which would lead to a decrease in the stability and bioavailability of DOPC[8]. Nevertheless,
696 the DPPC bilayer did not show the influence of unsaturated bonds, which made it more effective to be
697 synergistic regulated by SG and Dio.

698 In summary, we developed a novel and unique nanoliposome system, synergistically modulated by
699 structurally similar SG and Dio, to overcome the limitations of existing nanoliposome formulations. The
700 results showed that the synergistic effect of SG and Dio on DPPC nanoliposome (P-SG-Dio) could
701 significantly improve its stability, bioavailability and uric acid-lowering effect. Storage and
702 gastrointestinal tract stability experiments showed that minimal changes in physical and chemical
703 properties (including size, Dio retention) of P-SG-Dio compared to other formulations of nanoliposomes.
704 In cell experiments, P-SG-Dio had the highest cellular uptake and transepithelial transport capacity. Uric
705 acid-lowering assay showed that P-SG-Dio exhibits anti-hyperuricemia and anti-inflammatory effects by
706 effectively inhibiting the activation of NLRP3 inflammatory in the kidney. Therefore, this study provides
707 an innovative system with multiple functions for drug delivery, which has great potential for the

development of functional foods as well as different biomedical applications.

## ABBREVIATIONS USED

SG, sitogluside; Dio, dioscin; UA, uric acid; XOD, xanthine oxidase; NLRP3, NLR family pyrin domain containing3; BEN, Benzbromarone; Cho, cholesterol; DSC, differential scanning calorimetry; FTIR, fourier transform infrared spectroscopy; DiI, 1,1'-dioctadecyl-3,3,3',3'-tetramethylindocarbocyanine perchlorate; DPPC, 1,2-dipalmitoyl-sn-glycero-3-phosphocholine; DOPC, 1,2-dioleoyl-sn-glycero-3-phosphocholine; DOTAP, 1,2-dioleoyl-3-trimethylammoniumpropane; CCK-8, cell counting kit-8; DAPI, 4',6-diamidino-2-phenylindole; CRE, creatinine; BUN, blood urea nitrogen; MDA, malondialdehyde; SOD, superoxide dismutase; GSH-Px, glutathione peroxidase; ELISA, enzyme-linked immunosorbent assay; P-SG, DPPC-sitogluside; O-SG, DOPC-sitogluside; P-SG-Dio, DPPC-sitogluside-dioscin; O-SG-Dio, DOPC- sitogluside-dioscin; P-Cho-Dio, DPPC-cholesterol-dioscin; O-Cho-Dio, DOPC-cholesterol-dioscin; DLS, dynamic light scattering; TEM, transmission electron microscopy; EE, determination of encapsulation efficiency; DSC, differential scanning calorimetry; SGF, simulated gastric fluid; SIF, simulated intestinal fluid; OD, optical density; TEER, transepithelial electrical resistance; CMC-Na, carboxymethyl cellulose sodium; $P_{app}$, apparent permeability coefficient; SPF, pathogen free; HE, hematoxylin and eosin; IHC, Immunohistochemistry; RIPA, radioimmunoprecipitation assay; BCA, bicinchoninic acid; TBST, Tris-buffered saline/Tween; ECL, enhanced chemiluminescence; PDB, Protein Data Bank; GLUTs, glucose transporter proteins.

## NOTES

The authors declare no competing financial interest.

## ACKNOWLEDGMENTS

This work was supported by National Natural Science Foundation of China (32472367),

730 Zhejiang Province Natural Science Foundation (LGD22C200001) and the Key Research and
731 Development Program of Zhejiang province (2021C02019 & 2020C02046).

732 **SUPPORTING INFORMATION STATEMENT**

733 Order parameters of bare DPPC-DOTAP, P-SG, P-SG-Dio, DOPC-DOTAP, O-SG, O-SG-Dio
734 as deduced from Raman spectra; the standard curve of lucifer yellow; the effects of Dio liver injury.

735

## REFERENCES


(1) Ren, Q.; Tao, S.; Guo, F.; Wang, B.; Yang, L.; Ma, L.; Fu, P. Natural flavonol fisetin attenuated hyperuricemic nephropathy via inhibiting IL-6/JAK2/STAT3 and TGF-β/SMAD3 signaling. *Phytomedicine* **2021**, *87*, 153552. DOI: 10.1016/j.phymed.2021.153552.

(2) Lin, Y.; Liu, P. G.; Liang, W. Q.; Hu, Y. J.; Xu, P.; Zhou, J.; Pu, J. B.; Zhang, H. J. Luteolin-4′-O-glucoside and its aglycone, two major flavones of Gnaphalium affine D. Don, resist hyperuricemia and acute gouty arthritis activity in animal models. *Phytomedicine* **2018**, *41*, 54-61. DOI: 10.1016/j.phymed.2018.02.002.

(3) Chen, Y.; Li, C.; Duan, S.; Yuan, X.; Liang, J.; Hou, S. Curcumin attenuates potassium oxonate-induced hyperuricemia and kidney inflammation in mice. *Biomed Pharmacother* **2019**, *118*, 109195. DOI: 10.1016/j.biopha.2019.109195.

(4) Yang, B.; Xin, M.; Liang, S.; Huang, Y.; Li, J.; Wang, C.; Liu, C.; Song, X.; Sun, J.; Sun, W. Naringenin ameliorates hyperuricemia by regulating renal uric acid excretion via the PI3K/AKT signaling pathway and renal inflammation through the NF-κB signaling pathway. *J Agr Food Chem* **2023**, *71* (3), 1434-1446. DOI: 10.1021/acs.jafc.2c01513.

(5) Zhang, Y.; Jin, L.; Liu, J.; Wang, W.; Yu, H.; Li, J.; Chen, Q.; Wang, T. Effect and mechanism of dioscin from Dioscorea spongiosa on uric acid excretion in animal model of hyperuricemia. *J Ethnopharmacol* **2018**, *214*, 29-36. DOI: 10.1016/j.jep.2017.12.004.

(6) Li, R.; Zhang, L. Y.; Li, Z. J.; Xue, C. H.; Dong, P.; Huang, Q. R.; Wang, Y. M.; Zhang, T. T. Characterization and absorption kinetics of a novel multifunctional nanoliposome stabilized by sea cucumber saponins instead of cholesterol. *J Agr Food Chem* **2020**, *68* (2), 642-651. DOI: 10.1021/acs.jafc.9b06460.

(7) Baek, Y.; Jeong, E. W.; Lee, H. G. Encapsulation of resveratrol within size-controlled nanoliposomes: Impact on solubility, stability, cellular permeability, and oral bioavailability. *Colloid Surface B* **2023**, *224*, 113205. DOI: 10.1016/j.colsurfb.2023.113205.

(8) Liu, G.; Sun, P.; Yan, J.; Shao, P.; Feng, S. Regulation of nanoliposome rigidity and bioavailability of oligomeric proanthocyanidin with phytosterols containing different C3 branches. *Acs Appl Mater Inter* **2023**, *15* (37), 43414-43430. DOI: 10.1021/acsami.3c07854.

(9) Zhao, L.; Temelli, F.; Chen, L. Encapsulation of anthocyanin in liposomes using supercritical carbon dioxide: Effects of anthocyanin and sterol concentrations. *J Funct Foods* **2017**, *34*, 159-167. DOI: 10.1016/j.jff.2017.04.021.

(10) Yenigun, S.; Basar, Y.; Ipek, Y.; Gok, M.; Behcet, L.; Ozen, T.; Demirtas, I. A potential DNA protector, enzyme inhibitor and in silico studies of daucosterol isolated from six Nepeta species. *Process Biochem* **2024**, *143*, 234-247. DOI: 10.1016/j.procbio.2024.04.039.

(11) Zhu, Y.; Liang, J.; Gao, C.; Wang, A.; Xia, J.; Hong, C.; Zhong, Z.; Zuo, Z.; Kim, J.; Ren, H.; et al. Multifunctional ginsenoside Rg3-based liposomes for glioma targeting therapy. *J Control Release* **2021**, *330*, 641-657. DOI: 10.1016/j.jconrel.2020.12.036.

(12) Hong, C.; Liang, J.; Xia, J.; Zhu, Y.; Guo, Y.; Wang, A.; Lu, C.; Ren, H.; Chen, C.; Li, S.; et al. One Stone Four Birds: A novel liposomal delivery system multi-functionalized with ginsenoside Rh2 for tumor targeting therapy. *Nano-Micro Lett* **2020**, *12* (1), 129. DOI: 10.1007/s40820-020-00472-8.

(13) Han, C.; Yang, C.; Li, X.; Liu, E.; Meng, X.; Liu, B. DHA loaded nanoliposomes stabilized by β-sitosterol: Preparation, characterization and release *in vitro* and *vivo*. *Food Chem* **2022**, *368*, 130859. DOI: 10.1016/j.foodchem.2021.130859.

(14) Liu, S.; Lian, J.; Xu, Z.; Ning, Y.; Shi, M.; Zhao, Z.; Zhang, Z. Chitosan-coated nanoliposomes for

efficient delivery of betanin with enhanced stability and bioavailability. *Food Hydrocolloid* **2022**, *132*, 107871. DOI: 10.1016/j.foodhyd.2022.107871.

(15) Yang, M.; Lu, X.; Xu, J.; Liu, X.; Zhang, W.; Guan, R.; Zhong, H. Cellular uptake, transport mechanism and anti-inflammatory effect of cyanidin-3-glucoside nanoliposomes in Caco-2/RAW 264.7 co-culture model. *Front Nutr* **2022**, *9*, 995391. DOI: 10.3389/fnut.2022.995391.

(16) Li, F.; Dong, Y. Z.; Zhang, D.; Zhang, X. M.; Lin, Z. J.; Zhang, B. Molecular mechanisms involved in drug-induced liver injury caused by urate-lowering Chinese herbs: A network pharmacology study and biology experiments. *PloS one* **2019**, *14* (5), e0216948. DOI: 10.1371/journal.pone.0216948.

(17) Wohlert, M.; Benselfelt, T.; Wågberg, L.; Furó, I.; Berglund, L. A.; Wohlert, J. Cellulose and the role of hydrogen bonds: not in charge of everything. *Cellulose* **2022**, *29* (1), 1-23. DOI: 10.1007/s10570-021-04325-4.

(18) Hamedinasab, H.; Rezayan, A. H.; Mellat, M.; Mashreghi, M.; Jaafari, M. R. Development of chitosan-coated liposome for pulmonary delivery of N-acetylcysteine. *Int J Biol Macromol* **2020**, *156*, 1455-1463. DOI: 10.1016/j.ijbiomac.2019.11.190.

(19) Siapi, E.; Mavromoustakos, T.; Trandafir, V.; Albu, B.; Budrugeac, P. The use of differential scanning calorimetry to study the effects of gentamycin on fibrous collageneous membranes. *Thermochimica Acta* **2005**, *425* (1), 165-171. DOI: 10.1016/j.tca.2004.06.018.

(20) Et-Thakafy, O.; Delorme, N.; Gaillard, C.; Mériadec, C.; Artzner, F.; Lopez, C.; Guyomarc'h, F. Mechanical properties of membranes composed of gel-phase or fluid-phase phospholipids probed on liposomes by atomic force spectroscopy. *Langmuir* **2017**, *33* (21), 5117-5126. DOI: 10.1021/acs.langmuir.7b00363.

(21) Li, Q.; Lv, L.; Liu, Y.; Fang, Z.; Deng, Q.; Liang, W.; Wu, Y.; Chen, Z. Preparation, characterization

802 and application of bacteriocin CAMT6 nanoliposomes using resveratrol as a novel stabilizer. *Food Chem*
803 **2023**, *403*, 134293. DOI: 10.1016/j.foodchem.2022.134293.
804 (22) Cinelli, S.; Onori, G.; Zuzzi, S.; Bordi, F.; Cametti, C.; Sennato, S.; Diociaiuti, M. Properties of
805 mixed DOTAP-DPPC bilayer membranes as reported by differential scanning calorimetry and dynamic
806 light scattering measurements. *J Phys Chem B* **2007**, *111* (33), 10032-10039. DOI: 10.1021/jp071722g.
807 (23) Chen, Y.; Xia, G.; Zhao, Z.; Xue, F.; Gu, Y.; Chen, C.; Zhang, Y. 7,8-Dihydroxyflavone nano-
808 liposomes decorated by crosslinked and glycosylated lactoferrin: storage stability, antioxidant activity,
809 in vitro release, gastrointestinal digestion and transport in Caco-2 cell monolayers. *J Funct Foods* **2020**,
810 *65*, 103742. DOI: 10.1016/j.jff.2019.103742.
811 (24) Zhang, Y.; Pu, C.; Tang, W.; Wang, S.; Sun, Q. Effects of four polyphenols loading on the attributes
812 of lipid bilayers. *J Food Eng* **2020**, *282*, 110008. DOI: 10.1016/j.jfoodeng.2020.110008.
813 (25) Feng, S.; Sheng, J.; Yu, J.; Lin, Y.; Shao, P. Encapsulation and release of citral using nanostructured
814 lipid carriers: A study on the impact of different preparation methods. *Food Biosci* **2023**, *56*, 103185.
815 DOI: 10.1016/j.fbio.2023.103185.
816 (26) Pawlikowska-Pawlęga, B.; Misiak, L. E.; Zarzyka, B.; Paduch, R.; Gawron, A.; Gruszecki, W. I.
817 FTIR, 1H NMR and EPR spectroscopy studies on the interaction of flavone apigenin with
818 dipalmitoylphosphatidylcholine liposomes. *Biochim Biophys Acta Biomembr* **2013**, *1828* (2), 518-527.
819 DOI: 10.1016/j.bbamem.2012.10.013.
820 (27) Pu, C.; Tang, W.; Li, X.; Li, M.; Sun, Q. Stability enhancement efficiency of surface decoration on
821 curcumin-loaded liposomes: Comparison of guar gum and its cationic counterpart. *Food Hydrocolloid*
822 **2019**, *87*, 29-37. DOI: 10.1016/j.foodhyd.2018.07.039.
823 (28) Cong, L.; Wang, J.; Lu, H.; Tian, M.; Ying, R.; Huang, M. Influence of different anionic

polysaccharide coating on the properties and delivery performance of nanoliposomes for quercetin. *Food Chem* **2023**, *409*, 135270. DOI: 10.1016/j.foodchem.2022.135270.

(29) Sailer, K.; Viaggi, S.; Nüsse, M. Kinetics of radiation- and cytochrome c-induced modifications in liposomes analysed by FT–Raman spectroscopy. *Biochim Biophys Acta Biomembr* **1997**, *1329* (2), 259-268. DOI: 10.1016/S0005-2736(97)00113-2.

(30) Wang, L.; Huang, X.; Jing, H.; Ma, C.; Wang, H. Bilosomes as effective delivery systems to improve the gastrointestinal stability and bioavailability of epigallocatechin gallate (EGCG). *Food Res Int* **2021**, *149*, 110631. DOI: 10.1016/j.foodres.2021.110631.

(31) Ciorîță, A.; Suciu, M.; Macavei, S.; Kacso, I.; Lung, I.; Soran, M. L.; Pârvu, M. Green synthesis of Ag-$MnO_2$ nanoparticles using chelidonium majus and vinca minor extracts and their *in vitro* cytotoxicity. *Molecules* **2020**, *25* (4), 819. DOI: 10.3390/molecules25040819.

(32) Wang, G.; Wang, J. J.; Chen, X. L.; Du, L.; Li, F. Quercetin-loaded freeze-dried nanomicelles: Improving absorption and anti-glioma efficiency *in vitro* and *in vivo*. *J Control Release* **2016**, *235*, 276-290. DOI: 10.1016/j.jconrel.2016.05.045.

(33) Yang, M.; Lu, X.; Xu, J.; Liu, X.; Zhang, W.; Guan, R.; Zhong, H. Cellular uptake, transport mechanism and anti-inflammatory effect of cyanidin-3-glucoside nanoliposomes in Caco-2/RAW 264.7 co-culture model. *Front Nutr* **2022**, *9*, 995391. DOI: 10.3389/fnut.2022.995391.

(34) Kim, J. H.; Hong, S. S.; Lee, M.; Lee, E. H.; Rhee, I.; Chang, S. Y.; Lim, S. J. Krill oil-incorporated liposomes as an effective nanovehicle to ameliorate the inflammatory responses of DSS-induced colitis. *Int J Nanomedicine* **2019**, *14*, 8305-8320. DOI: 10.2147/ijn.S220053

(35) Alghurabi, H.; Tagami, T.; Ogawa, K.; Ozeki, T. Preparation, Characterization and *in vitro* evaluation of eudragit S100-coated bile salt-containing liposomes for oral colonic delivery of budesonide. *Polymers*

*(Basel)* **2022**, *14* (13), 2693. DOI: 10.3390/polym14132693.

(36) Elnaggar, Y. S. R.; Omran, S.; Hazzah, H. A.; Abdallah, O. Y. Anionic versus cationic bilosomes as oral nanocarriers for enhanced delivery of the hydrophilic drug risedronate. *Int J Pharm* **2019**, *564*, 410-425. DOI: 10.1016/j.ijpharm.2019.04.069.

(37) Meng, X.; Fryganas, C.; Fogliano, V.; Hoppenbrouwers, T. Double-coated nanoliposomes improve the bioavailability of flavanone hesperetin. *Food Hydrocolloid* **2024**, *151*, 109872. DOI: 10.1016/j.foodhyd.2024.109872.

(38) Roger, E.; Lagarce, F.; Garcion, E.; Benoit, J. P. Lipid nanocarriers improve paclitaxel transport throughout human intestinal epithelial cells by using vesicle-mediated transcytosis. *J Control Release* **2009**, *140* (2), 174-181. DOI: 10.1016/j.jconrel.2009.08.010.

(39) Wang, Y. F.; Zhang, C.; Yang, K.; Wang, Y.; Shan, S.; Yan, Y.; Dawson, K. A.; Wang, C.; Liang, X. J. Transportation of AIE-visualized nanoliposomes is dominated by the protein corona. *Natl Sci Rev* **2021**, *8* (6), nwab068. DOI: 10.1093/nsr/nwab068.

(40) Yi, X.; Shi, X.; Gao, H. J. Cellular uptake of elastic nanoparticles. **2011**, *107* (9), 098101. DOI: 10.1103/PhysRevLett.107.098101

(41) Xiang, S.; Sarem, M.; Shah, S.; Shastri, V. P. Liposomal treatment of cancer cells modulates uptake pathway of polymeric nanoparticles by altering membrane stiffness. *Small* **2018**, *14* (14), 1704245. DOI: 10.1002/smll.201704245.

(42) Csiszár, A.; Hersch, N.; Dieluweit, S.; Biehl, R.; Merkel, R.; Hoffmann, B. Novel fusogenic liposomes for fluorescent cell labeling and membrane modification. **2010**, *21* (3), 537-543. DIO:10.1021/bc900470y.

(43) Chen, Y.; Zhao, Z.; Li, Y.; Yang, Y.; Li, L.; Jiang, Y.; Lin, C.; Cao, Y.; Zhou, P.; Tian, Y.; et al.

Baicalein alleviates hyperuricemia by promoting uric acid excretion and inhibiting xanthine oxidase. *Phytomedicine* **2021**, *80*, 153374. DOI: 10.1016/j.phymed.2020.153374.

(44) Wang, N.; Li, P.; Pan, J.; Wang, M.; Long, M.; Zang, J.; Yang, S. *Bacillus velezensis* A2 fermentation exerts a protective effect on renal injury induced by Zearalenone in mice. *Sci Rep* **2018**, *8* (1), 13646. DOI: 10.1038/s41598-018-32006-z.

(45) Wang, M.; Lin, X.; Yang, X.; Yang, Y. Research progress on related mechanisms of uric acid activating NLRP3 inflammasome in chronic kidney disease. *Ren Fail* **2022**, *44* (1), 615-624. DOI: 10.1080/0886022X.2022.2036620.

(46) Wu, X.; Huang, R.; Ai, G.; Chen, H.; Ma, X.; Zhang, J.; Huang, Q.; Lao, J.; Zeng, H.; Li, C.; et al. 9-Hydroxy-8-oxypalmatine, a novel liver-mediated oxymetabolite of palmatine, alleviates hyperuricemia and kidney inflammation in hyperuricemic mice. *J Ethnopharmacol* **2024**, *335*, 118606. DOI: 10.1016/j.jep.2024.118606.

(47) Sharma, A.; Sharma, D.; Singh, M. Assessing Autonomic Level for Self-managed Systems – FAHP Based Approach. In *Advances in Computing and Data Sciences*, Singh, M., Gupta, P. K., Tyagi, V., Flusser, J., Ören, T., Eds.; Springer International Publishing: Cham, 2018; pp 114-123.

(48) Liang, X.; Mao, G.; Ng, K. Y. S. Mechanical properties and stability measurement of cholesterol-containing liposome on mica by atomic force microscopy. *J Colloid Interf Sci* **2004**, *278* (1), 53-62. DOI: 10.1016/j.jcis.2004.05.042.

(49) Silva, C.; Aranda, F. J.; Ortiz, A.; Martínez, V.; Carvajal, M.; Teruel, J. A. Molecular aspects of the interaction between plants sterols and DPPC bilayers: An experimental and theoretical approach. *Journal of Colloid and Interface Science* **2011**, *358* (1), 192-201. DOI: 10.1016/j.jcis.2011.02.048.

(50) Biswas, S.; Patil, P.; Ranjan, S.; Gautam, A. Exploring the therapeutic potential of dioscin and

diosgenin in neurological disorders. *Brain Behav Immun Integr* **2024**, *7*, 100069. DOI: 10.1016/j.bbii.2024.100069.

(51) Takechi-Haraya, Y.; Sakai-Kato, K.; Abe, Y.; Kawanishi, T.; Okuda, H.; Goda, Y. Atomic force microscopic analysis of the effect of lipid composition on liposome membrane rigidity. *Langmuir* **2016**, *32* (24), 6074-6082. DOI: 10.1021/acs.langmuir.6b00741.

(52) Rawicz, W.; Olbrich, K. C.; McIntosh, T.; Needham, D.; Evans, E. Effect of chain length and unsaturation on elasticity of lipid bilayers. *Biophys J* **2000**, *79* (1), 328-339. DOI: 10.1016/S0006-3495(00)76295-3.

**FIGURE CAPTIONS**

**Figure 1.** The effect of different ratio of SG to Dio on the fundamental features of DPPC or DOPC nanoliposomes, including particle size and PDI (A, B), ζ-potential (D, E), EE (G, H), appearance (C), size distribution and TEM image of P-SG-Dio (F) and O-SG-Dio (I), all the ratio of SG to Dio is 15:7.5, scale bars are 100 nm. DPPC: DPPC nanoliposomes with different ratio of SG to Dio. DOPC: DOPC nanoliposomes with different ratio of SG to Dio.

**Figure 2.** DSC thermograms of DPPC nanoliposomes (A) and DOPC nanoliposomes (B), Fourier transform infrared spectroscopy (FTIR) spectra of DPPC nanoliposomes (C) and DPPC nanoliposomes (D), Raman spectra of DPPC nanoliposomes (E) and DPPC nanoliposomes (F). All the ratio of SG to Dio is 15:7.5.

**Figure 3.** Effects of storage at different temperatures: 4 ℃ (A, D), 25 ℃ (B, E), and 37 ℃ (C, F) for 30 days on the Dio retention rate and particle size of nanoliposomes. The changes nanoliposome properties before and after simulated digestion: Dio release rate of P-SG-Dio and O-SG-Dio (G), as well as particle size (H), PDI (I) and ζ-potential (J) of P-SG, P-SG-Dio, O-SG and O-SG-Dio during *in vitro* simulated

912 gastrointestinal digestion for 6 h. All the ratio of SG to Dio is 15:7.5. Different capital letters represent
913 significant differences in the properties of different nanoliposomes at different stages of simulated
914 gastrointestinal tract digestion ($P < 0.05$). Different lower letters represent significant differences in the
915 properties of the same nanoliposomes at the same simulated gastrointestinal tract digestion stage ($P <$
916 0.05).

917 **Figure 4.** *In vitro* cytotoxicity study of P-SG, O-SG, Dio-loaded nanoliposomes, SG solution, Dio
918 solution and SG/Dio mix solution against Caco-2 cells (A); CLSM images of the cellular uptake of P-
919 SG, O-SG and Dio-loaded nanoliposomes in Caco-2 cells, blue represented nuclei stained with 4′,6-
920 diamidino-2-phenylindole (DAPI) and red represented DiI-labeled nanoliposomes, the scale bars are 40
921 μm (B); mean fluorescence intensity of P-SG, O-SG, Dio-loaded nanoliposomes associated with Caco-2
922 cells detected by flow cytometry (C); TEER values of Caco-2 cells with time (n = 3 times) (D); alkaline
923 phosphatase activity (n = 3 times per group), different capital letters represent significant differences in
924 enzyme activity of AP and BL on days 7, 14 and 21 ($P < 0.05$); different lower letters represent significant
925 differences in enzyme activity of AP and BL on the same day ($P < 0.05$) (E); transport across Caco-2
926 monolayers of Dio, Dio-loaded nanoliposomes, $P_{app}$ value of from AP to BL side across Caco-2
927 monolayers (cm/s) (n=3 times per group) (F).

928 **Figure 5.** Effects of Dio-loaded nanoliposomes on mice with hyperuricemia. Average water consumption
929 (A), body weight (B), serum XOD (C), liver XOD (D), serum UA (E), serum BUN, serum Cr (SCr),
930 kidney index (H), affected renal (%) (I), micrographs of renal H&E staining (J). The representative
931 pictures of kidney histopathology (200×, 400×). Data are showed as mean ± S.E.M of 8 mice in each
932 group.

933 **Figure 6.** Effects of Dio-loaded nanoliposomes on the levels of pro-inflammatory cytokines. Serum IL-

934 1β (A), kidney IL-1β (B), serum IL-18 (C), kidney IL-18 (D), serum MDA (E), serum SOD (F), serum
935 GSH-Px (G), the relative of IL-1β level in kidney (H), the representative IHC pictures of IL-1β in kidney
936 (200×, 400×) (n = 8) (I). Data are showed as mean ± S.E.M of 8 mice in each group.
937 **Figure 7.** Effects of Dio-loaded nanoliposomes on NLRP3 inflammasome signal pathway expressions
938 in hyperuricemic mice. The protein expressions of NLRP3 (A), ASC (B), caspase1 (C) and IL-1β (D)
939 were quantitated by Image software. The protein expressions of NLRP3, ASC, caspase1 and IL-1βwere
940 detected by Western blot in kidney tissue (E). The mRNA expression of NLRP3 (F), ASC (G), caspase1
941 (H) and IL-1β (I) in kidney tissue were detected by RT-PCR. Data are showed as mean ± S.E.M of 8 mice
942 in each group.

**Table 1. Primer sequences.**

| Name of primer | Primer sequences |
|---|---|
| IL-1β | Forward, 5'-GCCCATCCTCTGTGACTCA-3′ |
| | reverse, 5'-AGTTGTCTGATTCCAGGTCTCCAT-3' |
| ASC | forward, 5'-AGACATGGGCTTACAGGA-3' |
| | reverse, 5'-CTCCCTCATCTTGTCTTGG-3' |
| Caspase1 | forward, 5'-TATCCAGGAGGAATATGTG-3' |
| | reverse, 5'-ACAACACCACTCCTTGTTTC-3' |
| NLRP3 | forward, 5'-GTGGTGACCCTCTGTGAGGT-3' |
| | reverse, 5'-TCTTCCTGGAGCGCTTCTAA-3' |
| β-actin | forward, 5'-GGTCATCACTATTGGCAACG-3' |
| | reverse, 5'-ACGGATGTCAACGTCACACT-3' |

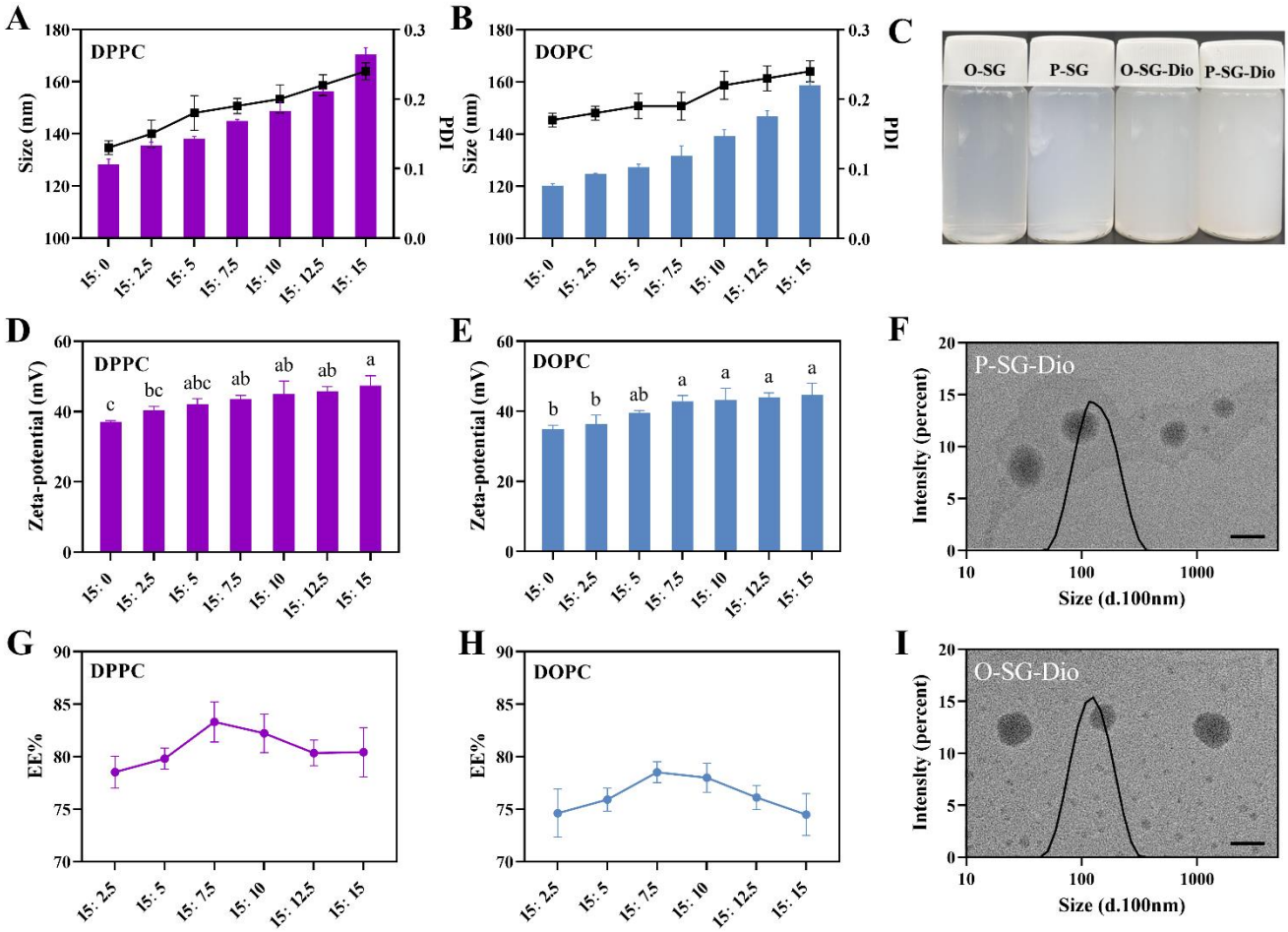
A
DPPC
Size (nm)
PDI
B
DOPC
C
O-SG
P-SG
O-SG-Dio
P-SG-Dio
D
DPPC
Zeta-potential (mV)
c
bc
abc
ab
ab
ab
a
E
DOPC
b
b
ab
a
a
a
a
F
P-SG-Dio
Intensity (percent)
Size (d.100nm)
G
DPPC
EE%
H
DOPC
I
O-SG-Dio
15: 0
15: 2.5
15: 5
15: 7.5
15: 10
15: 12.5
15: 15

**Figure 1**

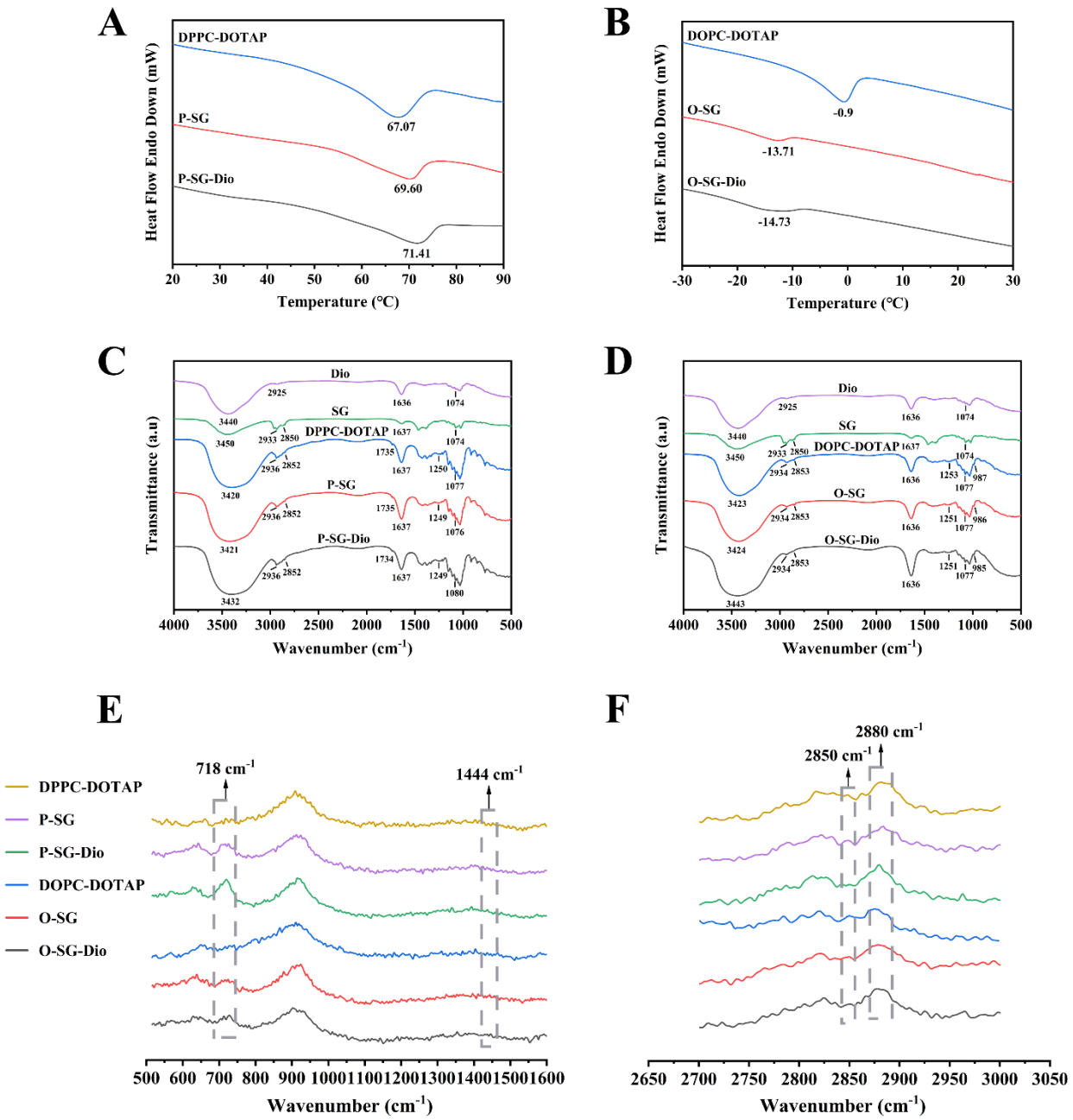
A
DPPC-DOTAP
P-SG
P-SG-Dio
67.07
69.60
71.41
Heat Flow Endo Down (mW)
Temperature (°C)
B
DOPC-DOTAP
O-SG
O-SG-Dio
-0.9
-13.71
-14.73
Heat Flow Endo Down (mW)
Temperature (°C)
C
Dio
SG
DPPC-DOTAP
P-SG
P-SG-Dio
Transmittance (a.u)
Wavenumber (cm-1)
D
Dio
SG
DOPC-DOTAP
O-SG
O-SG-Dio
Transmittance (a.u)
Wavenumber (cm-1)
E
718 cm-1
1444 cm-1
DPPC-DOTAP
P-SG
P-SG-Dio
DOPC-DOTAP
O-SG
O-SG-Dio
Wavenumber (cm-1)
F
2880 cm-1
2850 cm-1
Wavenumber (cm-1)

**Figure 2**

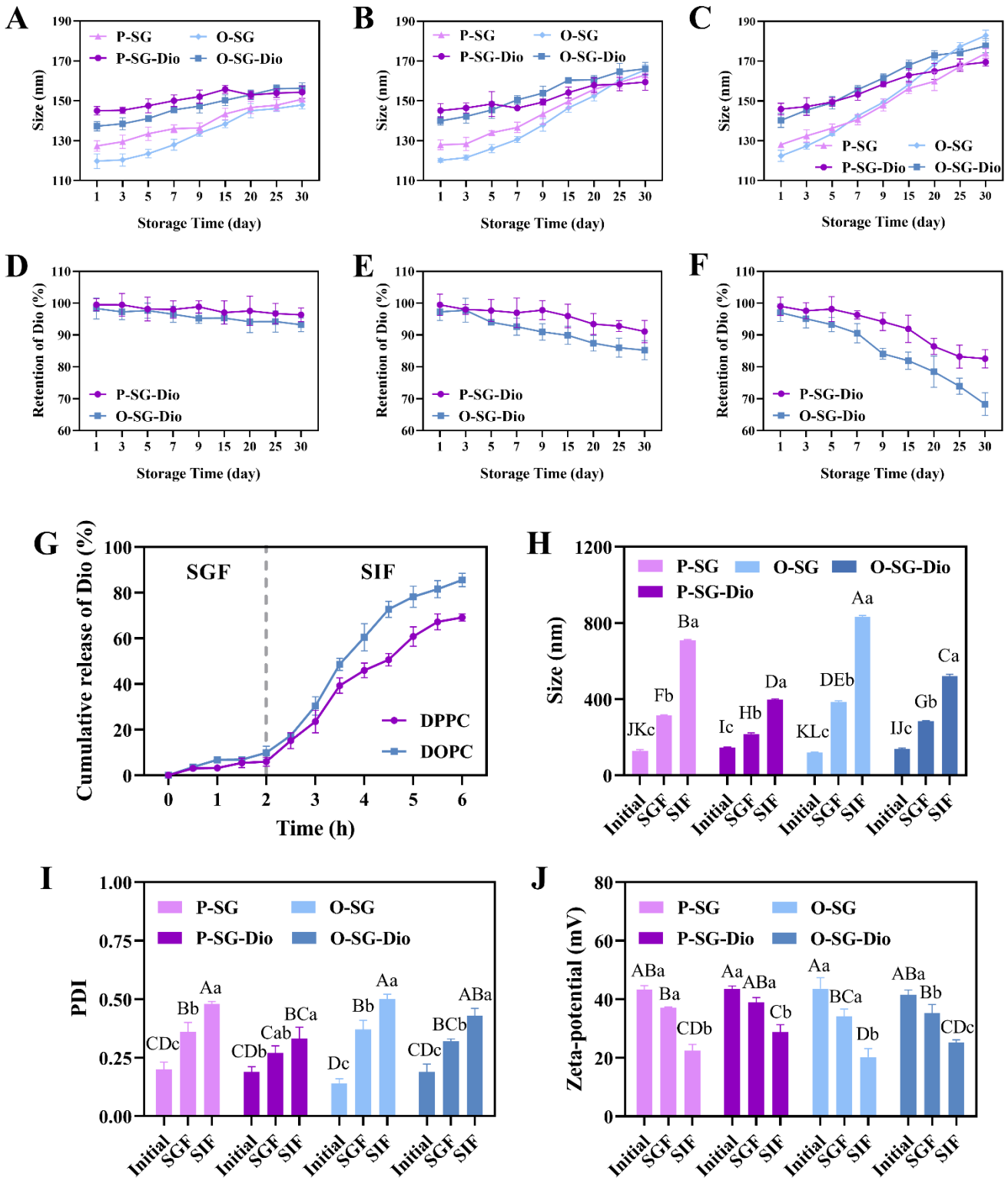
A
B
C
D
E
F
G
H
I
J
P-SG
O-SG
P-SG-Dio
O-SG-Dio
Size (nm)
Storage Time (day)
Retention of Dio (%)
Cumulative release of Dio (%)
SGF
SIF
DPPC
DOPC
Time (h)
PDI
Zeta-potential (mV)
Initial
SGF
SIF

Figure 3

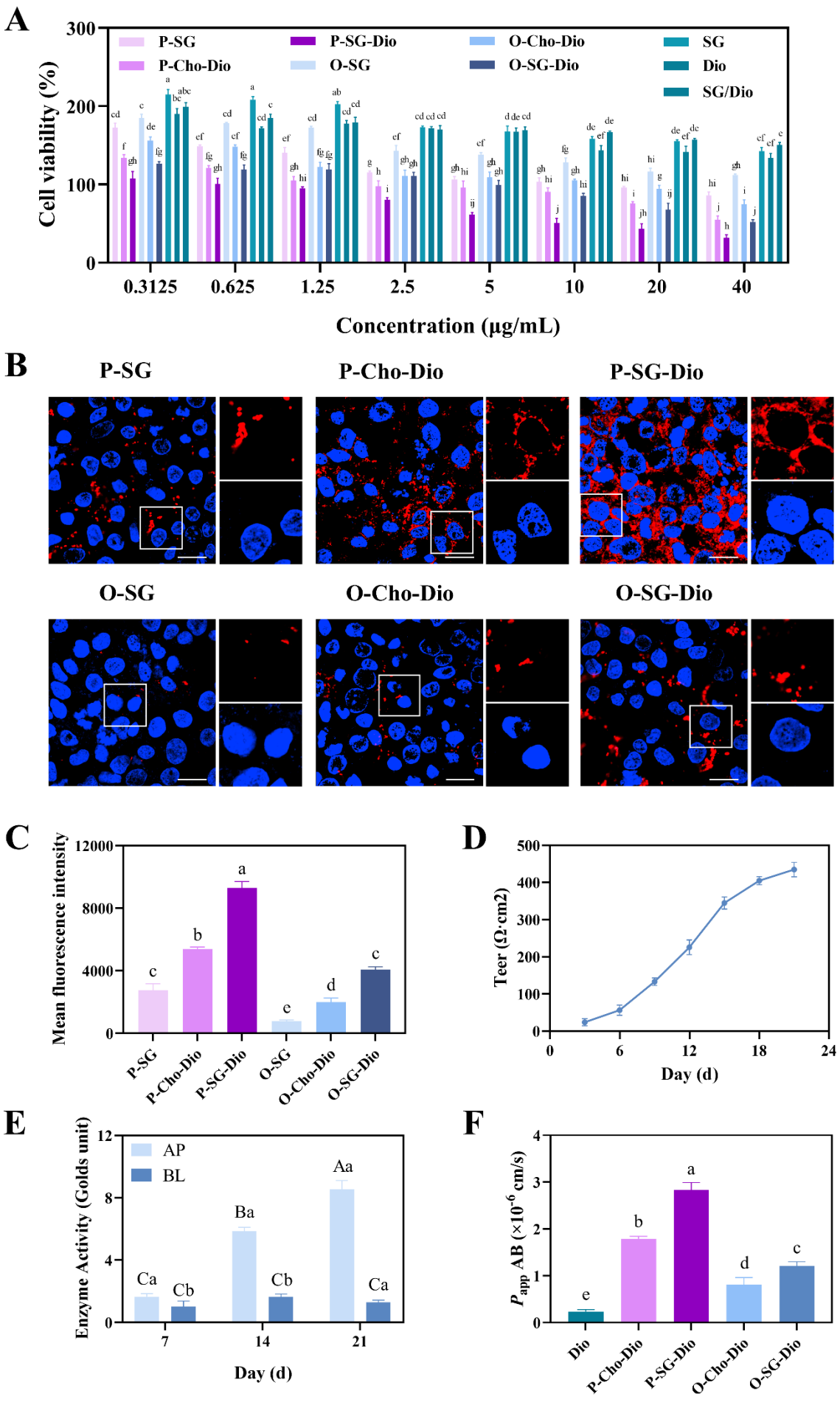
A
Cell viability (%)
P-SG
P-Cho-Dio
P-SG-Dio
O-SG
O-Cho-Dio
O-SG-Dio
SG
Dio
SG/Dio
Concentration (μg/mL)
B
P-SG
P-Cho-Dio
P-SG-Dio
O-SG
O-Cho-Dio
O-SG-Dio
C
Mean fluorescence intensity
D
Teer (Ω·cm2)
Day (d)
E
Enzyme Activity (Golds unit)
AP
BL
Day (d)
F
$P_{app}$ AB (×10$^{-6}$ cm/s)
Dio
P-Cho-Dio
P-SG-Dio
O-Cho-Dio
O-SG-Dio

Figure 4

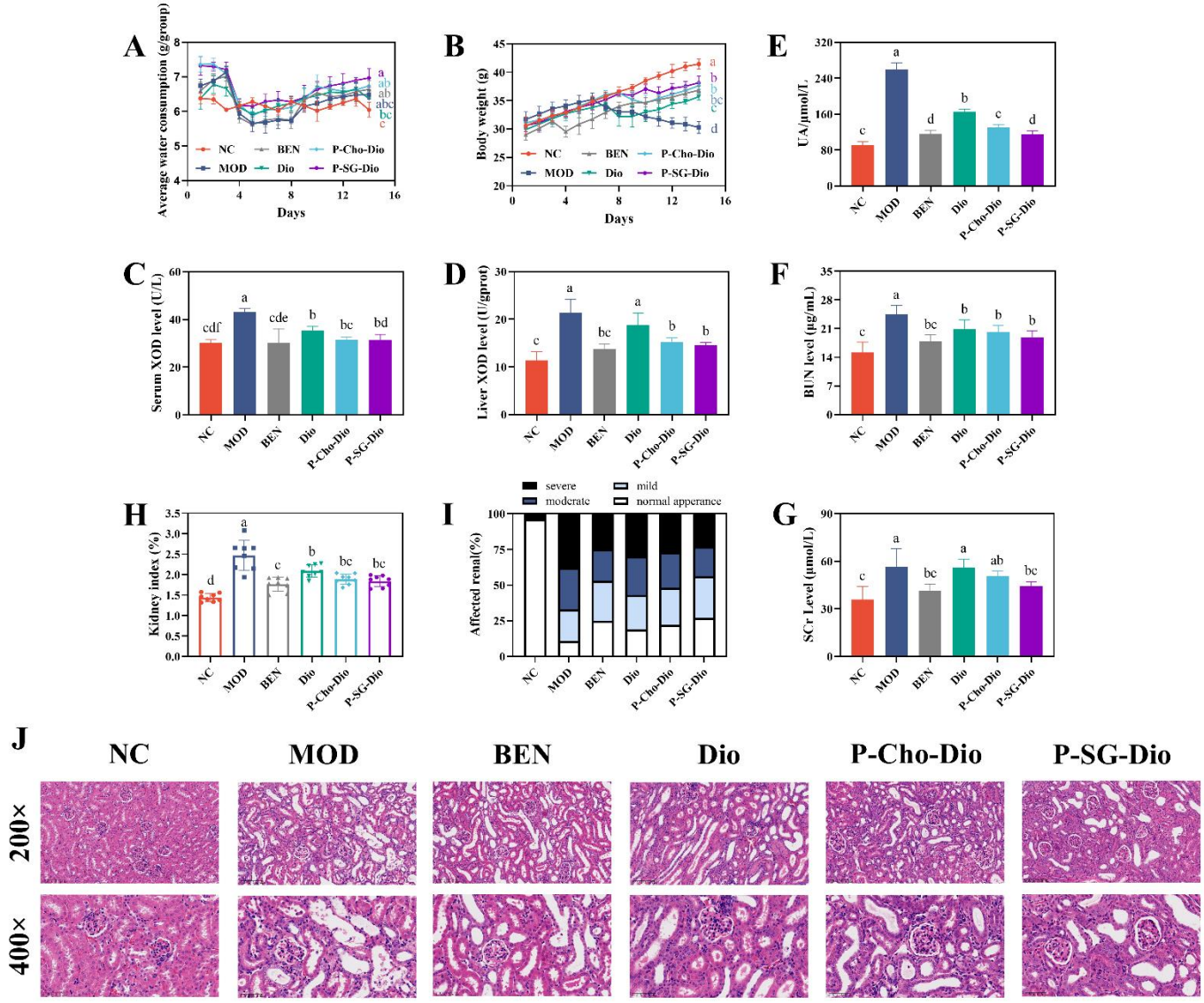
A
Average water consumption (g/group)
Days
NC
MOD
BEN
Dio
P-Cho-Dio
P-SG-Dio
B
Body weight (g)
Days
E
UA/μmol/L
C
Serum XOD level (U/L)
D
Liver XOD level (U/gprot)
F
BUN level (μg/mL)
H
Kidney index (%)
I
Affected renal(%)
severe
moderate
mild
normal apperance
G
SCr Level (μmol/L)
J
NC
MOD
BEN
Dio
P-Cho-Dio
P-SG-Dio
200×
400×

**Figure 5**

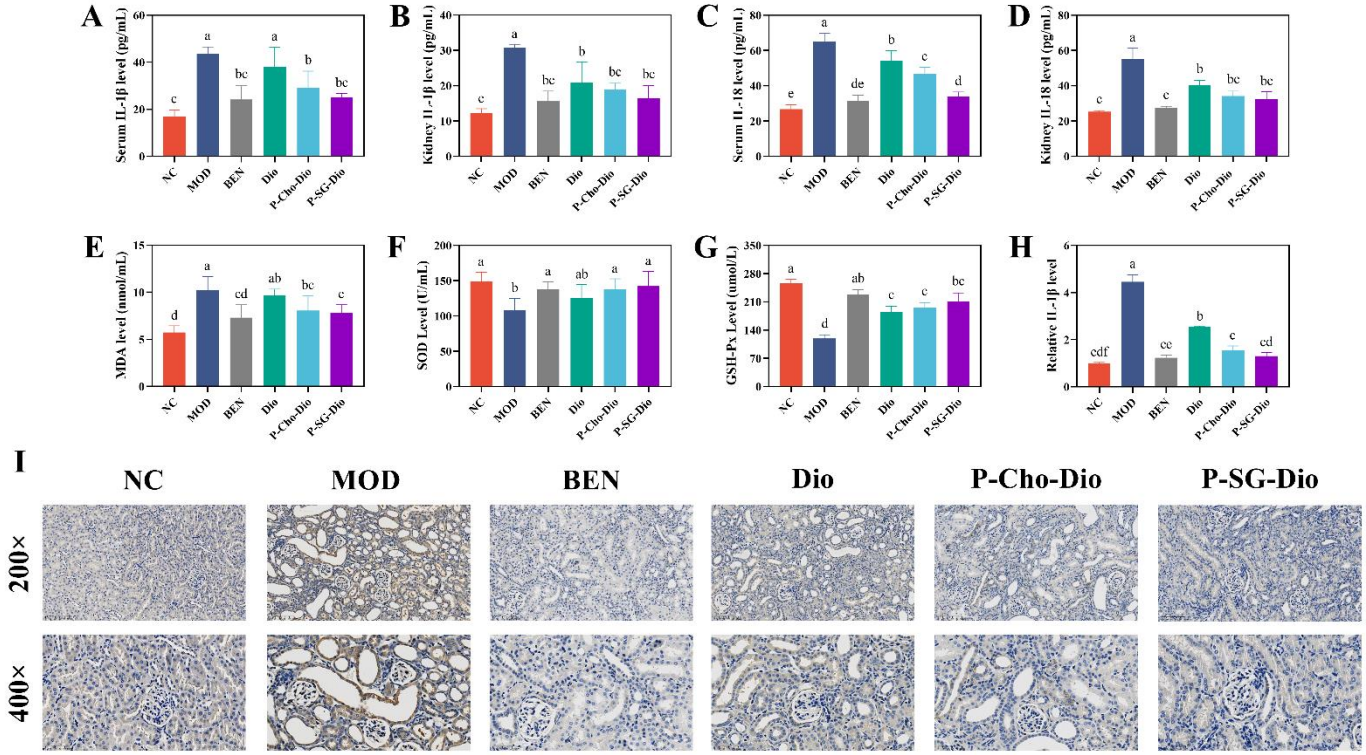
A
Serum IL-1β level (pg/mL)
B
Kidney IL-1β level (pg/mL)
C
Serum IL-18 level (pg/mL)
D
Kidney IL-18 level (pg/mL)
E
MDA level (nmol/mL)
F
SOD Level (U/mL)
G
GSH-Px Level (umol/L)
H
Relative IL-1β level
NC
MOD
BEN
Dio
P-Cho-Dio
P-SG-Dio
I
200×
400×

**Figure 6**

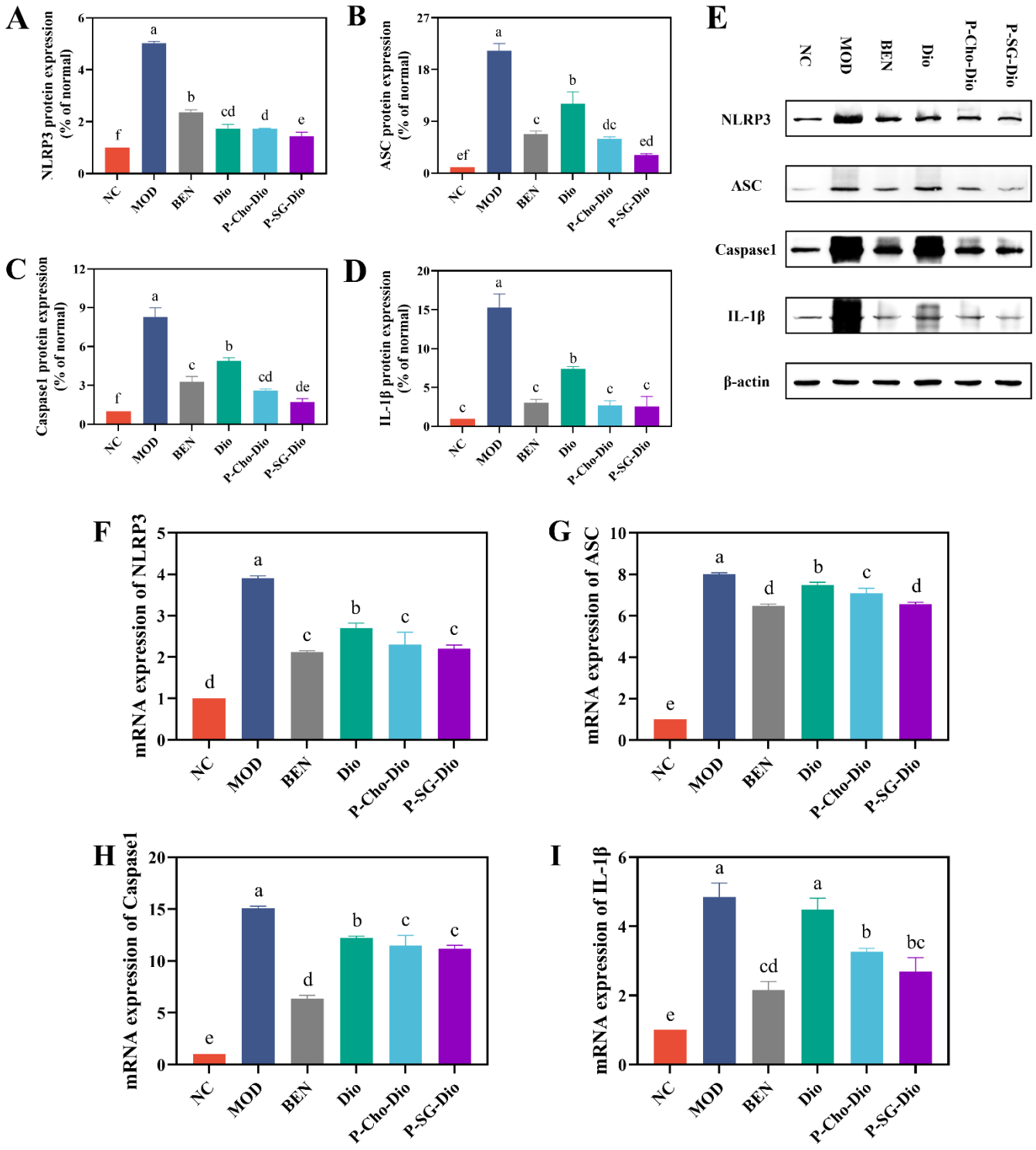
A
NLRP3 protein expression (% of normal)
B
ASC protein expression (% of normal)
C
Caspase1 protein expression (% of normal)
D
IL-1β protein expression (% of normal)
E
NC
MOD
BEN
Dio
P-Cho-Dio
P-SG-Dio
NLRP3
ASC
Caspase1
IL-1β
β-actin
F
mRNA expression of NLRP3
G
mRNA expression of ASC
H
mRNA expression of Caspase1
I
mRNA expression of IL-1β

**Figure 7**

**TOC graphic (For Table of Contents Only)**